RECONSTRUCTION OF EARLY PALEOGENE NORTH PACIFIC DEEP-WATER CIRCULATION USING THE NEODYMIUM ISOTOPIC COMPOSITION OF FOSSIL FISH DEBRIS

A Thesis

by

ASHLEY MELISSA HAGUE

Submitted to the Office of Graduate Studies of
Texas A&M University
in partial fulfillment of the requirements for the degree of

MASTER OF SCIENCE

August 2011

Major Subject: Oceanography

Reconstruction of Early Paleogene North Pacific Deep-Water Circulation Using the Neodymium Isotopic Composition of Fossil Fish Debris

RECONSTRUCTION OF EARLY PALEOGENE NORTH PACIFIC DEEP-WATER CIRCULATION USING THE NEODYMIUM ISOTOPIC COMPOSITION OF FOSSIL FISH DEBRIS

A Thesis

by

ASHLEY MELISSA HAGUE

Submitted to the Office of Graduate Studies of
Texas A&M University
in partial fulfillment of the requirements for the degree of

MASTER OF SCIENCE

Approved by:

Chair of Committee, Deborah J. Thomas
Committee Members, Robert L. Korty
Mitchell W. Lyle
Head of Department, Piers Chapman

August 2011

Major Subject: Oceanography

ABSTRACT

Reconstruction of Early Paleogene North Pacific Deep-Water Circulation Using the Neodymium Isotopic Composition of Fossil Fish Debris. (August 2011)
Ashley Melissa Hague, B.S., Indiana University of Pennsylvania
Chair of Advisory Committee: Dr. Deborah J. Thomas

To better understand the operating mode of the deep oceans during fundamentally warm climate intervals, we present new Nd isotope data from Deep Sea Drilling Project and Ocean Drilling Program sites in the North Pacific to expand the reconstruction of water mass composition and structure during the early Cenozoic. Fossil fish debris from Sites 192, 464, 465, 883, 884 and 1208 (paleowater depths spanning 900 to 4000 m) were used to reconstruct the water mass composition from ~85 to 30 Ma.

The fish debris is shown to not be overprinted as there was no systematic offset between the detrital silicate and the fish debris composition. Cleaned and uncleaned fish debris were both included in the reconstruction of water mass composition as they were found to record the same Nd isotope composition.

North Pacific deep water convection occurred from ~67 to 45 Ma, the peak in production is recorded by broadly coincident trends at Sites 192, 464 and 883. Further support for North Pacific deep-water convection during the early Paleogene are the geographic trends in detrital silicate versus fish debris composition, greater separation at the more northerly Emperor Seamount sites, and the location of the most radiogenic detrital values at the Emperor Seamount sites. The Emperor Seamount chain likely played a major role in the flow of the North Pacific deep-water mass as it acted as a physical barrier to flow at deep-water sites compared to shallow depths (albeit still deep-water). ε_{Nd} values indicate the timing of the cessation of major, deep convection in the North Pacific occurred much earlier, ~52 Ma than the timing obtained from shallower Shatsky Rise

sites, ~45 Ma. Convection in the North Pacific likely produced a dense water mass that influenced the deeper sites in this study more than the shallower sites until ~52 Ma when convection was not as intense or the waters were not sufficiently dense to impact the deeper sites. Deep water convection was most intense during the relatively "cool" portion of the Late Cretaceous and Early Paleocene.

For Grandma Hoffman

ACKNOWLEDGEMENTS

First and foremost, I owe the greatest thanks to my advisor, Debbie Thomas, who has always been there supporting and guiding me on my journey. Thank you for your quick edits and valuable input on this work. Also, thank you to my committee members, Rob Korty and Mitch Lyle, for their valuable advice. I also wouldn't be where I am today without the experience and guidance provided by Steve Hovan, at Indiana University of Pennsylvania, while working on my undergraduate research.

A special thank you goes to Dan Murphy and Stella Woodard, for their generous teaching and guidance in the radiogenic clean lab. Also, thank you to Brent Miller for always assisting with the TIMS and to Jennifer Hertzberg for keeping me on track when I thought I couldn't keep going.

Finally, to my family who has always believed in me, I cannot thank you enough. To Mom and Dad whose support is endless and pride is ever growing. Thank you to Brandy who was there every day to tell me that it all happens for a reason. To Tawny, Larry, Kayla, Natalie and Mallory who were always a phone call away to brighten my day. And to Scott, thank you for your continuous support. I love you all.

NOMENCLATURE

Elements

Fe	Iron
Mn	Manganese
Nd	Neodymium
Pb	Lead
REE	Rare Earth Element
Sm	Samarium

Units

Ma	Million years ago
mbsf	meters below sea floor
Myr	Million years
pg	picogram
pmol	picomole
ppm	parts per million
μm	microns
μL	microliter

Water Masses

AABW	Antarctic Bottom Water
AAIW	Antarctic Intermediate Water
CDW	Circumpolar Deep Water
NADW	North Atlantic Deep Water

Other

CC	Core Catcher
CCD	Carbonate Compensation Depth

CHUR	Chondritic Uniform Reservoir
DSDP	Deep Sea Drilling Project
FO	First Occurrence
ITCZ	Intertropical Convergence Zone
LO	Last Occurrence
MOC	Meridional Overturning Circulation
ODP	Ocean Drilling Program
SST	Sea Surface Temperature
TIMS	Thermal Ionization Mass Spectrometer

TABLE OF CONTENTS

LIST OF FIGURES

LIST OF TABLES

1. INTRODUCTION

A growing body of neodymium (Nd) and lead (Pb) isotopic data from ferromanganese crusts and fossil fish debris (biogenic apatite) is beginning to provide a reconstruction of ancient Pacific Ocean intermediate- and deep-water masses in order to address the role of deep ocean circulation on climate during the early Paleogene greenhouse interval. Relatively little is known about how and where deep waters formed during this interval of time due to the different boundary conditions, tectonic settings (e.g., oceanic gateways) and the thermal structure of the atmosphere and oceans.

Recent Nd isotopic data suggests that a bipolar mode of meridional overturning circulation (MOC) may have operated in the Pacific during a portion of the early Cenozoic. Nd isotopic data from the Paleogene tropical Pacific, Ocean Drilling Program (ODP) Sites 1209 and 1211, suggest a contribution of waters from the North Pacific mixed with waters derived from the South Pacific [*Thomas*, 2004]. The onset of the deep-water contribution from the North Pacific began ~65 Ma, lasted about ~20 Myr, and then diminished by ~45 Ma [*Thomas*, 2004]. *Thomas et al.* [2008] investigated ODP Sites 1215, 1217, 1219 and 1221, and these data contributed more details of the geographic and vertical extent of the hypothesized water masses, but also revealed a more complicated reconstruction. One fundamental challenge in reconstructing the details of Pacific water mass distribution is that the current body of Pacific Nd isotopic data all derives from sites located in a limited geographical region in the tropical Pacific. Additional data from locations closer to the possible region of deepwater formation must be investigated to fully assess the possibility of a Pacific bipolar MOC during the early Paleogene.

This thesis follows the style of *Paleoceanography*.

In this thesis we generated new Nd isotopic data from fossil fish debris to expand the reconstruction of water mass composition and structure during the early Paleogene. The focus of this work is the North Pacific, adding records from Deep Sea Drilling Project (DSDP) and ODP Sites 192, 464, 465, 883, 884, and 1208, therefore extending the existing geographic coverage of Nd isotopic data north to 40°N paleolatitude (Site 192) (Figure 1). Site 192 is the closest site available to a possible region of North Pacific deep-water formation. The goal of this reconstruction is to understand the operating mode of the deep oceans during greenhouse climates with the ultimate goal of determining the role of deep ocean circulation in global heat transport during fundamentally warm climate intervals.

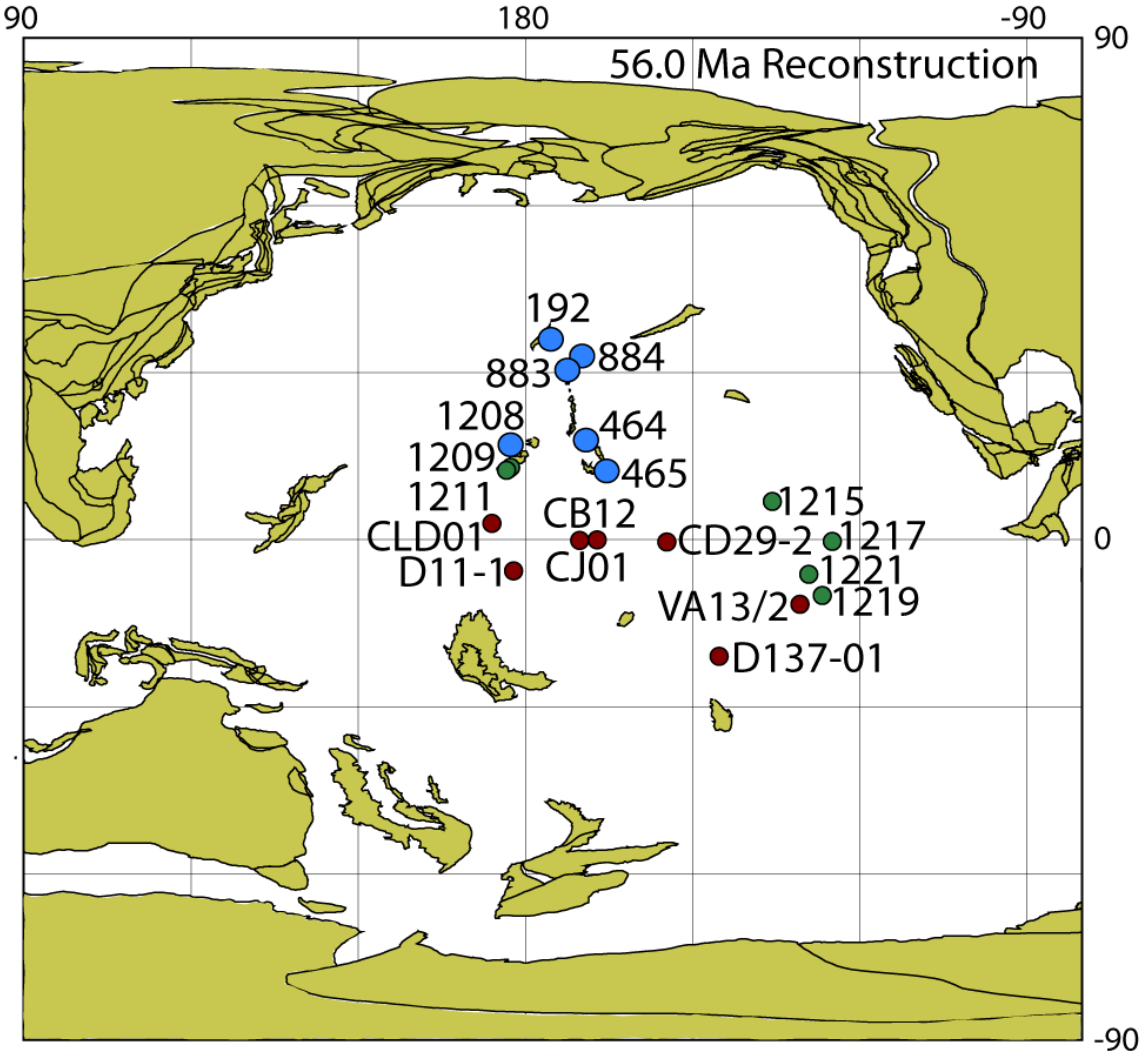

Figure 1. Paleogeographic reconstruction - 56.0 Ma. Location of ferromanganese (Fe-Mn) crusts indicated by red circles and DSDP and ODP site locations: published data - green circles, this study - blue circles. (modified from the Ocean Drilling Stratigraphic Network www.odsn.de)

2. BACKGROUND

2.1 *Modern Thermohaline Circulation*

Thermohaline circulation is driven by density gradients, and is responsible for a large proportion of heat transport from the equator to the poles as well as ventilation of the deep ocean basins [e.g., *Broecker*, 1997]. Deep water is formed in a few locations where cold, dense water sinks at high latitudes and then advects through the ocean basins at depth. In the modern oceans, water sinks at high-latitudes in the Atlantic and Southern Oceans to form the principal deep-water masses. Surface waters from the Gulf Stream that are warm and saline ultimately sink as cold, saline North Atlantic Deep Water (NADW) due to intense cooling in the Labrador and Greenland-Iceland-Norwegian (GIN) Seas. NADW flows south where it upwells in the Antarctic divergence. Some of the upwelled NADW is mixed into and re-sinks as part of Antarctic Bottom Water (AABW), while some portion advects north to the Antarctic Convergence and subducts as part of Antarctic Intermediate Water (AAIW). Circumpolar Deep Water (CDW), flows into the deep portions of the Indian and Pacific oceans. Deep convection in the modern regime does not occur in the North Pacific as it does in the North Atlantic and Southern Ocean due to low North Pacific surface water salinities [e.g., *Levitus*, 1982]. Furthermore, dense bottom water cannot enter the North Pacific from the Arctic region due to the shallow Bering Strait sill [*Tomczak and Godfrey*, 1994].

2.2 *Early Paleogene Climate*

Early Paleogene (~65 to 45 Ma) climate was significantly warmer than modern conditions and is considered to be the most recent major greenhouse interval in Earth history. During this time high latitude sea surface temperatures (SSTs), reconstructed from oxygen isotopes, were at least 10°C [*Stott et al.*, 1990] and Arctic SSTs, reconstructed from TEX_{86} and dinocyst analyses, were 15-18°C [*Sluijs et al.*, 2006]. Comparison of high latitude SSTs to those reconstructed for the tropics, 28-32°C [e.g., *Pearson et al.*, 2001], indicate the equator-to-pole temperature gradient during the early

Paleogene was roughly half the modern gradient. Warmer SSTs at higher latitudes implies enhanced heat transport from the tropics, however, this process is at odds with the lower temperature gradient between high and low latitudes, which should slow meridional heat transport. An additional consideration in trying to understand ocean-climate dynamics during the early Cenozoic is that surface-to-deep water temperature gradients were also significantly reduced as benthic foraminiferal $\delta^{18}O$ values report bottom-water temperatures of 8-12°C [*Zachos et al.*, 2001]. As a consequence, the operating mode of the deep oceans and its role in global heat transport during fundamentally warm climate intervals is not well understood.

2.3 *Early Paleogene Paleogeography*

Paleogeographic reconstructions of the early Paleogene indicate continental and oceanic basin configurations were substantially different from the modern (Figure 2). During the early Cenozoic the Arctic-North Atlantic basins were more restricted. The Norwegian and Greenland Seas did not open until the late Paleocene/early Eocene, ~55 Ma [*Saunders et al.*, 1997; *Moran et al.*, 2006]; therefore, deep water could not have formed there as during the Holocene. Because of the different geometry, potential North Atlantic deep water formation sites lay within a latitude band of 50-60°N in the early Paleogene, versus 65-75°N in the Holocene. Furthermore, the Tethyan and Caribbean seaways were still open, connecting the Atlantic and Pacific oceans at lower latitudes, but the Tasman Sea and Drake Passage were not open yet to deep flow [*Frakes and Kemp*, 1972; *Lawver and Gahagan*, 2003]. The Pacific during the early Paleogene also was larger than the modern Pacific and proportionately larger than the Atlantic at that time. Thus, at least from a paleogeographic perspective, the Pacific likely had a proportionately greater influence on and role in climate dynamics during the early Paleogene than the other basins.

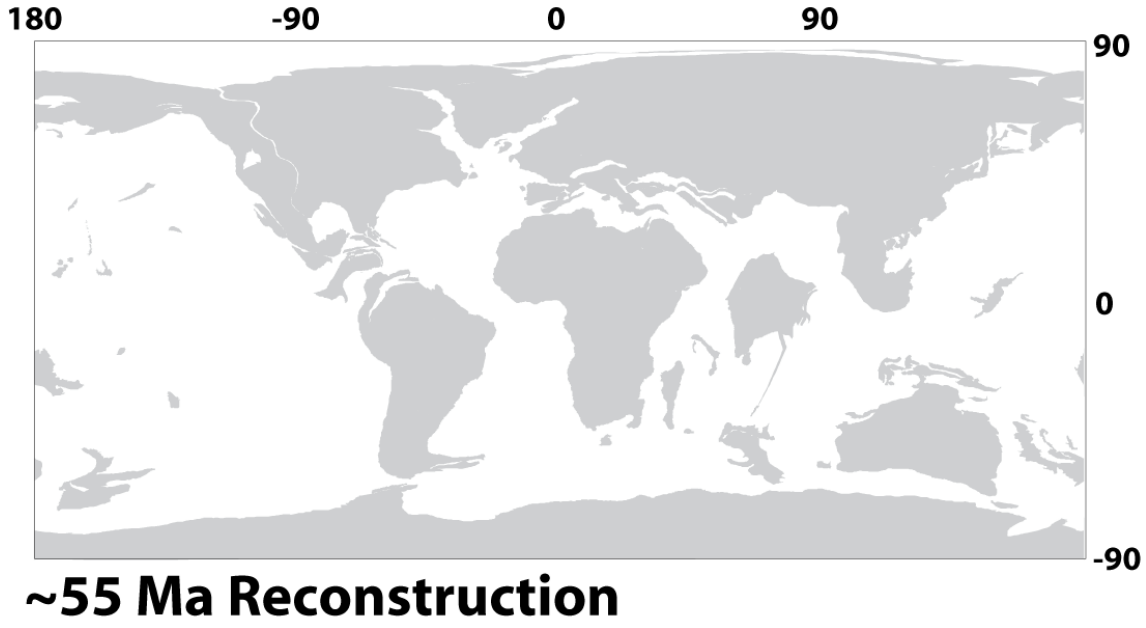

Figure 2. Paleogeographic reconstruction - 55.0 Ma. Paleogene continental and oceanic basin configurations were substantially different from the modern. (modified from the Ocean Drilling Stratigraphic Network www.odsn.de)

2.4 *Neodymium Isotope Tracer of Water Mass Composition*

Nd is a light rare earth element (REE) with seven naturally occurring isotopes (^{142}Nd, ^{143}Nd, ^{144}Nd, ^{145}Nd, ^{146}Nd, ^{148}Nd, and ^{150}Nd). ^{143}Nd is produced by the α-decay of ^{147}Samarium (Sm) (half life of 1.06×10^{11} years), while ^{144}Nd is stable and not radiogenic. All REE are incompatible (prefer the melt phase); however, light REE are more incompatible than heavy REE. Therefore, Nd fractionates from Sm during partial melting of the mantle, concentrating Sm in the mantle [eg., *DePaolo and Wasserburg*, 1976]. Thus, rocks from the depleted mantle yield a higher Sm/Nd ratio than continental crust, which are enriched in light REE. Therefore, the isotopic composition of the crust varies due to the age, degree of melting, and the minerals that comprise the constituent rocks. Rocks with a high Sm/Nd ratio also yield a high (more radiogenic) ^{143}Nd/^{144}Nd ratio because they contain higher initial concentrations of the parent. Consequently, basalts contain more radiogenic ^{143}Nd/^{144}Nd values than older, granitic formations.

Nd isotopic ratios are expressed in epsilon notation (ε_{Nd}). The sample $^{143}Nd/^{144}Nd$ ratio is normalized to the average value of the bulk earth, the Chondritic Uniform Reservoir (CHUR):

$$\varepsilon_{Nd} = \{[(^{143}Nd/^{144}Nd_{\ sample})/(^{143}Nd/^{144}Nd_{\ CHUR})]-1\} \text{ X } 10^4,$$

where the present day value of CHUR is 0.512638 [*DePaolo and Wasserburg*, 1976]. The ε_{Nd} value of ancient samples must be corrected for in situ production of ^{143}Nd from the decay of ^{147}Sm after incorporated into sample, and such age corrected values are expressed as $\varepsilon_{Nd}(t)$:

$$\varepsilon_{Nd}(t) = \{[(^{143}Nd/^{144}Nd_{\ initial\ sample})/(^{143}Nd/^{144}Nd_{\ t\ CHUR})]-1\} \text{ X } 10^4,$$

where CHUR is the ratio at a given time *t* in the past.

Fluvial inputs are the primary source of dissolved Nd load to the oceans [*Elderfield and Greaves*, 1982; *Goldstein and Jacobsen*, 1987; *Goldstein and Jacobsen*, 1988; *Halliday et al.*, 1992; *Jones et al.*, 1994; *Amakawa et al.*, 2000]. Hydrothermal input of dissolved Nd is negligible due to removal by hydrothermal scavenging [*Halliday et al.*, 1992] and eolian contributions to the dissolved inventory of Nd in the oceans also are negligible [*Jones et al.*, 1994]. Fluvial inputs to a given region of the surface ocean reflect an average of the different source rocks weathered within the particular drainage system [*Goldstein and Jacobsen*, 1988; *Amakawa et al.*, 2000]. As the residence time of Nd in the oceans is short, ~500 to 1000 years, [e.g., *Tachikawa et al.*, 1999], relative to global oceanic mixing, ~1500 years [*Broecker et al.*, 1960], inter- and intra-basinal differences in isotopic composition exist. The surface water Nd signal is exchanged with underlying water masses, intermediate and deep, in regions of deep-water ventilation [*Goldstein and Jacobsen*, 1988; *Elderfield et al.*, 1990; *Halliday et al.*, 1992, *Sholkovitz*, 1993]. The Nd isotopic signature of waters below the thermocline largely reflect the isotopic composition of the dissolved Nd delivered to the intermediate- and deep-water mass source region [eg., *Piepgras and Wasserburg*, 1982; *Piepgras and Wasserburg*, 1987; *Piepgras and Jacobsen*, 1988; *Bertram and Elderfield*, 1993; *Jeandel*, 1993; *Jeandel et*

al., 1998; *Amakawa et al.*, 2000]. The initial Nd signal of an intermediate- or deep-water mass can be altered by water mass mixing during advection away from the source, but the provenance information is retained and can therefore be utilized as a tracer of deep-ocean circulation. Fractionation by biological or low-temperature processes does not have any effect on the Nd isotopic composition [*Goldstein and Hemming*, 2003]; it will only become altered when mixed with another source consisting of different isotopic composition [*Amakawa et al.*, 2000]. Deep-water Nd isotopic values at a given location may vary due to changes in weathering and runoff inputs into areas of deep-water formation [*Elderfield and Greaves*, 1982; *Goldstein and Jacobsen*, 1988; *Halliday et al.*, 1992; *Jones et al.*, 1994], changes in the circulation pattern of deep waters, changes in water mass mixing [e.g., *Piepgras and Wasserburg*, 1982, 1987; *Piepgras and Jacobson*, 1988; *Jeandel*, 1993; *Shimizu et al.*, 1994; *Jeandel et al.*, 1998; *von Blanckenburg*, 1999; *Amakawa et al.*, 2000; *Goldstein et al.*, 2007], particle exchange [e.g. *Goldstein and Hemming*, 2003] and boundary exchange [e.g. *Lacan and Jeandel*, 2001, 2005a; *Zhang et al.*, 2008].

Variations in the deep-water Nd isotopic composition reflect the age and composition of the terrain weathered into the water mass formation region. The surface waters of the North Pacific are the most radiogenic ε_{Nd} values (~0 to -4) [*Piepgras and Wasserburg*, 1982; *Piepgras and Jacobsen*, 1988; *Shimizu et al.*, 1994] due to an average fluvial input of -2.9 to -3.7 [*Goldstein and Jacobsen*, 1988]. This is due to the weathering of young, circum-Pacific arc volcanics [e.g., *Stordal and Wasserburg*, 1986; *Goldstein and Jacobsen*, 1987; *Goldstein and Jacobsen*, 1988; *Piepgras and Jacobsen*, 1988; *Goldstein and Hemming*, 2003; *Amakawa et al.*, 2004; *Lacan and Jeandel*, 2005a]. The surface waters of portions of the South Pacific are radiogenic (~0) with lower values (~-8) at 4500 m depth [*Piepgras and Wasserburg*, 1982] due to the northward flow of AABW (~-9) [*Piepgras and Jacobsen*, 1988], indicating greater stratification than the North Pacific. Although three distinct water masses are present in the North Pacific (intermediate water, deepwater and bottom water), Nd isotopic compositions are slightly

more negative at depth, but are not as stratified as they are in the South Pacific [e.g., *Tomczak and Godfrey*, 1994]. An AABW signature is not evident in North Pacific deep-water due to a slow deepwater renewal, the "North Pacific" deep and bottom water signatures derive from particle exchange with the intermediate radiogenic surface water. It is important to note that modern North Pacific deep waters acquire their Nd isotopic signature due to particle scavenging and exchange, and not deep-water convection. The initial less radiogenic AABW signature is overprinted by particle scavenging and exchange with radiogenic inputs along the deep water path, there is no input that is less radiogenic than the inflowing AABW.

Fossil fish teeth and bones (biogenic apatite) record and retain the Nd isotopic composition of the seawater in which they are deposited [e.g., *Shaw and Wasserburg*, 1985; *Staudigel et al.*, 1985; *Reynard et al.*, 1999]. Fish debris is useful for paleoceanographic investigations of ancient water mass Nd because of its widespread geographic and abundant stratigraphic distribution, offering the potential to generate high-resolution records [*Martin and Scher*, 2004]. *Thomas and Via* [2007] showed that fish bones and debris record and preserve the same signal as fossil fish teeth. The seawater Nd isotopic composition is recorded in biogenic apatite at the sediment-water interface [e.g., *Staudigel et al.*, 1985; *Reynard et al.*, 1999]; therefore, the signal recorded in the biogenic apatite is that of the water bathing the seafloor [e.g., *Wright et al.*, 1984; *Shaw and Wasserburg*, 1985; *Staudigel et al.*, 1985; *Martin and Haley*, 2000]. As the teeth and bones of living fish contain no REE and there is no metabolic uptake of Nd during the fish's lifetime, the life habits of the fish have no bearing on the Nd signal recorded [e.g., *Wright et al.*, 1984, *Staudigel et al.*, 1985]. Biogenic apatite, $Ca_5(PO_4,CO_3)_3OH$ or carbonate hydroxylapatite, has a small crystal structure in living bone and teeth [*Person et al.*, 1995; *Martin et al.*, 2005]. The carbonate hydroxylapatite recrystallizes during an early diagenetic reaction to flourapatite ($Ca_5(PO_4)_3F$), which is thermodynamically stable at seafloor temperatures. During this early diagenetic reaction at the sea floor, REE are incorporated into the biogenic apatite lattice and locked in as

the crystal grows around them [*Armstrong et al.*, 2001], resulting in high concentrations of Nd (100-1000ppm) [*Wright et al.*, 1984; *Shaw and Wasserburg*, 1985; *Staudigel et al.*, 1985]. The concentration of Nd in fish teeth (100-1000 ppm) is ~ six orders of magnitude greater than the Nd composition of seawater (10s of pmol) [*Elderfield and Greaves*, 1982]. Biogenic apatite is resistant to dissolution in corrosive bottom waters and subsequent burial diagenesis [*Staudigel et al.*, 1985; *Elderfield and Pagett*, 1986; *Grandjean et al.*, 1987; *Martin and Haley*, 2000; *Martin and Scher*, 2004], and only during high-grade metamorphism can alteration occur [*Person et al.*, 1995].

2.5 *Previous Studies –Early Paleogene Deep Ocean Circulation*

An investigation of Nd isotopic records from the northwest tropical Pacific, ODP Sites 1209 and 1211 (Figure 1), produced evidence that a bipolar mode of MOC operated in the Pacific during the early Paleogene (Figure 3) [*Thomas*, 2004]. ε_{Nd} values at both sites increased from relatively non-radiogenic values (~-4 to -5), to higher values (~-3) by ~63 Ma. The higher values persisted at both sites for ~20 Myr then shifted back to relatively non-radiogenic values (~-4 to -5) by ~40 Ma. The shift to higher ε_{Nd} values from ~65 to ~40 Ma suggests an increase in the influence of waters from the North Pacific, perhaps from actual convection of deep waters in the North Pacific. The shift to a North Pacific source, suggested by the ε_{Nd} trend, occurred during the warmest conditions of the Cenozoic (Figure 3). Furthermore, the Nd and $\delta^{18}O$ records show the onset of the shift in deep-water production lags the warming and the switch back to a Southern Ocean source occurs with the global cooling. However, it is important to note that ferromanganese records south of Sites 1209 and 1211 show no indication of a North Pacific deep-water mass contribution [*Ling et al.*, 1997; *van de Flierdt et al.*, 2004].

Thomas et al. [2008] investigated ODP Leg 199 Sites 1215, 1217, 1219, and 1221 (Figure 1) to further investigate if the tropical Pacific was the mixing location of water from the Southern Ocean and the North Pacific Ocean the details of which are described below. The new data corroborated a bimodal MOC during the early to middle Paleogene. The Leg 199 ε_{Nd} values range from -3.5 to -5.5 with no distinctive trends

over the time span recorded at each site. However, the consistency of the data, with the majority of the ε_{Nd} values between ~-4 to -5, suggests that Leg 199 sites were bathed by a common deepwater mass that extended from ~2800 to 4500 m. The Leg 199 sites recorded lower values than at Shatsky Rise, suggesting the two locations may have been bathed by different deepwater masses from ~56 to 42 Ma. After ~45 Ma a common deepwater mass may have bathed Shatsky Rise sites and Leg 199 sites, as Shatsky values became less radiogenic. Overall, from ~65 to 45 Ma the North Pacific water mass circulated south to the Southern High of Shatsky Rise sites (paleolatitude ~10-15˚N) at depths of ~2400 m (Site 1209) to 2900 m (Site 1211). From 53.6 to 49.3 Ma Site 1215 values were much closer to the lower limit of Shatsky, suggesting a maximum southern extent for the North Pacific deepwater. However, as 1215 lies to the east and backtracks ~6° south of Shatsky Rise, the geographic influence of the North Pacific deep water mass may have ended between Shatsky Rise and Site 1215. Until 53.6 Ma, the Southern Ocean deepwater mass circulated northward in the western part of the basin from ~1800 m (Crust D11-1) to abyssal depths and to ~10°N paleolatitude (Site 1215). Also, the fact that the deep tropical Pacific ε_{Nd} values remained more radiogenic than -6 throughout the Paleogene indicates a lack of Atlantic deep water influence via the Caribbean Seaway.

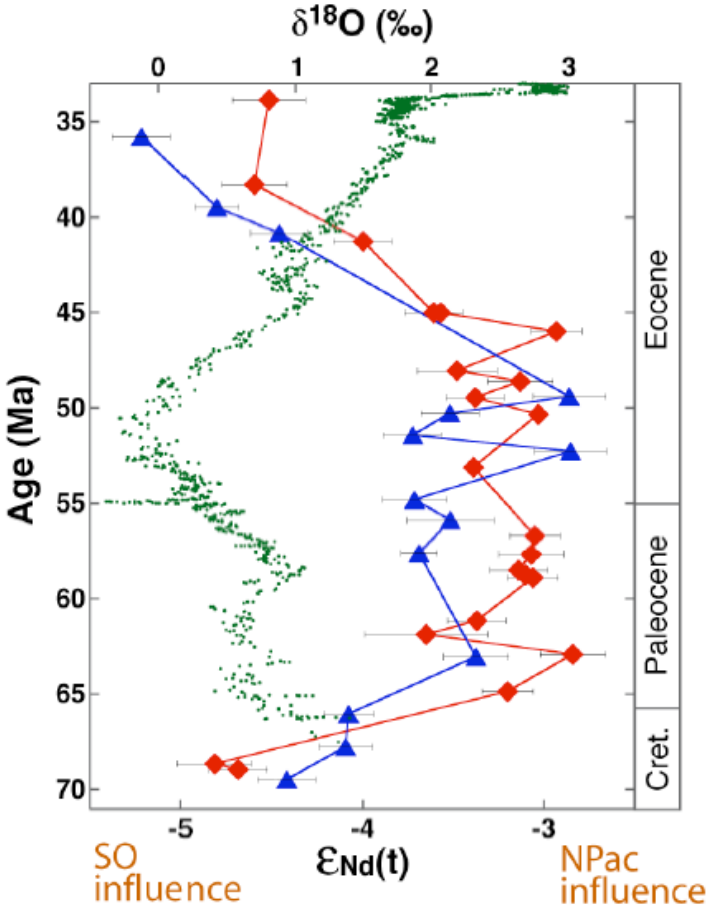

Figure 3. Nd isotopic data from Shatsky Rise. Site 1209 (red) and 1211 (blue) indicate a switch in the source region of Pacific deep-water. The shift to a North Pacific source in the $\varepsilon_{Nd}(t)$ trend is within the warmest deep-sea conditions of the Cenozoic, $\delta^{18}O$ (green). (from *Thomas*, 2004)

3. SAMPLES AND METHODS

3.1 *Study Sites*

Information for all study sites can be located in Table 1. Paleolatitudes are from the site locations at ~56 Ma as shown in Figure 1.

Table 1. Details of the sites investigated.

Site	**192 A**	**464**	**465**
Location	Meiji Guyot	Northern Hess Rise	Southern Hess Rise
Paleolatitude	40°N	18°N	12°N
Paleodepth	2500 m	4000 m	900 m
Top of Section	Core 1	Core 5	Core 2
Bottom of Section	Core 4	Core 9	Core 10
Youngest Age	Late Eocene	Late Eocene	Late Paleocene
Oldest Age	Maastrichtian	Late Cretaceous	Late Maastrichtian
Site	**465 A**	**883 B**	**884 B**
Location	Southern Hess Rise	Detroit Seamount	Detroit Seamount
Paleolatitude	12°N	32°N	32°N
Paleodepth	900 m	2000 m	3300 m
Top of Section	Core 1	Core 75	Core 74
Bottom of Section	Core 5	Core 87	Core 90
Youngest Age	Late Paleocene	Late Eocene	Late Eocene
Oldest Age	Late Maastrichtian	Maastrichtian	Early Eocene
Site	**1208**		
Location	Central Shatsky Rise		
Paleolatitude	15°N		
Paleodepth	3300 m		
Top of Section	Core 36		
Bottom of Section	Core 41		
Youngest Age	Late Oligocene		
Oldest Age	Late Cretaceous		

Site 192: Hole 192 A is located on Meiji Guyot on the northwestern end of the Emperor Seamount chain, paleowater depth of 2500 m and paleolatitude 40˚N. The stratigraphic

section spanning the study interval was recovered in cores 1 through 4 in Hole 192 A. The lithology is predominately nannofossil chalk and calcareous claystone.

Site 464: Located on the northern end of Hess Rise, paleowater depth of 4000 m and paleolatitude 18˚N. The stratigraphic section spanning the study interval was recovered in cores 5 through 9. The lithology is predominately pelagic brown clay barren of calcareous microfossils.

Site 465: Hole 465 and Hole 465 A are located on the southern end of Hess Rise, paleowater depth of 900 m and paleolatitude 12˚N. The stratigraphic section spanning the study interval was recovered in cores 2 through 10 in Hole 465 and cores 1 through 5 in Hole 465 A. The lithology is predominately nannofossil ooze and foraminifera - nannofossil ooze, with chert and calcite crystals common throughout the section.

Site 883: Hole 883 B is located on Detroit Seamount, paleowater depth of 2000 m and paleolatitude 32˚N. The stratigraphic section spanning the study interval was recovered in cores 75 through 87. The lithology is predominately a nannofossil chalk with abundant altered volcanic ash toward the base of the studied section.

Site 884: Hole 884 B is located on Detroit Seamount, paleowater depth of 3300 m and paleolatitude 32˚N. The stratigraphic section spanning the study interval was recovered in cores 74 through 90 and the sediments are predominately chalk, conglomerate and claystone with altered ash.

Site 1208: Hole 1208 A is located on the Central High of Shatsky Rise, paleowater depth of 3300 m and paleolatitude 15˚N. The stratigraphic section spanning the study interval was recovered in cores 36 through 41 and consisted of claystone.

The above DSDP and ODP sites extend the geographic coverage of the proxy-based reconstructions of water mass chemistry in the North Pacific to higher latitudes, Sites 192, 883 and 884. The new water mass composition data from Hess Rise, Sites 464 and 465, provide a useful complement to existing data from Shatsky Rise, located at a similar paleolatitude. Furthermore, inclusion of the deeper Shatsky Rise Site 1208 enables us to determine if the waters bathing Sites 1209 and 1211 extended to deep-water depths.

3.2 *Age Models*

Age models were constructed for each site using available published biostratigraphic datums and linearly interpolating between them. Sources of the published datums and applied numeric ages from timescales are listed in each site's respective description and table. Many of the DSDP and ODP sites investigated lack age control due to a paucity of preserved microfossils and/or detailed study of the sections. Below, the construction of each site's age model is described.

Site 192: Shipboard nannofossil identification published in the Leg 19 Initial Reports for Site 192 [*Creager et al.*, 1973] (pages 542-548) were assigned numeric ages from *Gradstein et al.* [2004]. The K/T boundary identified in Core 4 CC is used as the bottom datum [*Creager et al.*, 1973] (page 473). We placed the boundary at the top of the core catcher (CC), 1024 mbsf , and assigned a numeric age from *Gradstein et al.* [2004]. As there is no CC photo the stratigraphic position of the K/T boundary is a bit arbitrary, however our placement is consistent with shipboard identification of the mid-Maastrictian in the middle of the CC. See Table 2 for datum information.

Table 2. Datums for Site 192 age model.

Site 192			
	Depth	Nannofossil Zone	Age (Ma)
Core	(mbsf)	*Creager et al.* [1973]	*Gradstein et al.* [2004]
Top 1	942.00	top NP 22	32.40
Bottom 1	951.00	base NP 19	36.20
Top 2	951.00	top NP 18	36.20
Bottom 3	989.00	base NP 17	39.60
Top 4	1018.00	top NP 14	46.60
4 CC	1024.00	K/T Boundary	65.50

Site 464: Essentially no biostratigraphic age control exists for the clay interval investigated from Site 464 [*Thiede et al.*, 1981]. Thus we used the highest datum below the clay interval and the lowest datum above the clay interval as the primary age control tie points. The shipboard scientists assigned an age of 75 Ma to the oldest brown clay at the base of Section 10, 89.00 meters below seafloor (mbsf) [*Thiede et al.*, 1981] (page 164). The upper tie point was particularly problematic. We used the first occurrence of the radiolarian *S. pentas* (32.00 mbsf, 2.80 Ma) for the youngest age model tie point. The bottom of Section 4 (32.00 mbsf) is shown as the base of radiolarian *S. pentas* in *Thiede et al.* [1981] (page 168). *Theyer and Hammond* [1974] list the base of *S. pentas* and *Stichocorys peregrina* as the same zonal boundary and *Gradstein et al.* [2004] assigned the LO *Stichocorys peregrina* as 2.8 Ma. By linearly interpolating between the two datums listed above, age model calculations using Pliocene radiolarian datums and late Miocene diatom and silicoflagellate datums resulted in ages too young (i.e., no sample older than late Paleocene) conflicting with the ichthyolith stratigraphy, which nominally identified the Cretaceous/Paleogene boundary within core 8 (between sections 8-2 and 9-1). It is not possible to convert the ichthyolith "datums" directly to accurate ages due to the low sampling resolution as well as the coarse age resolution of the biostratigraphy itself. Arbitrarily assigning numerical ages and specific subseafloor depths to the "datums" is just as imprecise as linear interpolation between only three datums. Thus, we opted to have a middle datum (50.00 mbsf, 55.80 Ma) based on the most precisely identified ichthyolith age. The middle datum was assigned using the

Paleocene-Eocene boundary age from *Gradstein et al.* [2004] and by splitting the depth difference between the base of *Doyle and Riedel* [1981] sample 6-5, 74-80 and the top of sample 7-1, 70-77. This resulted in a distribution of ages throughout the section consistent with the qualitative age assignments of *Doyle and Riedel* [1981]. See Table 3 for datum information.

Table 3. Datums for Site 464 age model.

Site 464 Core	Depth (mbsf)	Source	Datum	Age (Ma)	Source
Base 4	32.00	*Thiede et al.* [1981]	*S. pentas*	2.80	*Gradstein et al.* [2004]
Base 6	50.00	*Doyle and Riedel* [1981]	Paleocene /Eocene	55.80	*Gradstein et al.* [2004]
Base 10	89.00	*Thiede et al.* [1981]	oldest brown clay	75.00	*Thiede et al.* [1981]

Site 465 (Hole 465 and 465 A): Biostratigraphic datums were not published for this site; however, sub-bottom depths (m) and ages (Ma) were published in the Leg 62 Initial Reports for Site 465 and 465 A [*Rea and Harrsch*, 1981] (page 665). As more than one sample depth was listed with 57.0 and 58.0 Ma, the depths were averaged for that age. As the biostratigraphic markers were not listed we were unable to update the ages as in *Gradstein et al.* [2004]. See Table 4 for datum information.

Table 4. Datums for Site 465 age model.

Site 465			
Rea and Harrsch [1981]			
Sample (Core, Section, Interval)	Sub-bottom Depth (m)	Average Depth (m)	Age (Ma)
1-1, 76-78	0.77		1.00
2-2, 64-68	3.15		2.50
2-5, 64-66	7.65		4.00
3-1, 60-62	11.11		55.00
3-3, 60-62	14.11		56.00
4-2, 48-50	21.99	26.31	57.00
4-4, 48-50	24.99		57.00
5-2, 95-97	31.96		57.00
5-5, 95-97	36.46	38.63	58.00
6-2, 28-30	40.79		58.00
6-4, 28-30	43.79		59.00
10-2, 30-32	78.81		65.00
10-5, 30-32	83.31		66.00

Table 5. Datums for Site 465 A age model.

Site 465 A		
Rea and Harrsch [1981]		
Sample (Core, Section, Interval)	Sub-bottom Depth (m)	Age (Ma)
1-1, 132-134	40.33	58.00
3-2, 18-20	59.69	64.50
3-5, 18-20	64.69	66.00

Site 883: The stratigraphic position of calcareous nannofossil datums in the Leg 145 Initial Reports for Site 883 [*Rea et al.*, 1993] (page 140-141) were used to create this age model. As depth intervals were listed in top and bottom depths, the numerical age from *Gradstein et al.* [2004] were applied to the mean depth of the datum from *Rea et al.* [1993]. Some datums were not included as the biomarker datum was not located in *Gradstein et al.* [2004] or depth intervals were missing in *Rea et al.* [1993]. Also, as some datum mean depths were the same, the age was averaged between the two depths. See Table 6 for datum information.

Table 6. Datums for Site 883 age model.

Site 883					
Biomarker Datum *Rea et al.* [1993]	Top Depth (mbsf)	Bottom Depth (mbsf)	Mean (mbsf)	Age (Ma) *Gradstein et al.* [2004]	Ave (Ma)
LO *Discoaster barbadienis*	712.60	720.10	716.35	34.40	35.30
FO *Isthmolithus recurvus*	712.60	720.10	716.35	36.20	
LO *Chiasmolithus solitus*	729.90	739.70	734.80	39.80	-
FO *Discoaster sublodoensis*	779.20	789.20	784.20	48.80	50.00
LO *Tribrachiatus orthostylus*	779.20	789.20	784.20	51.20	
FO *Discoaster lodoensis*	813.40	814.70	814.05	52.60	-
FO *Discoaster mohleri*	814.70	828.10	821.40	58.40	58.90
FO *Heliolithus kleinpellii*	814.70	828.10	821.40	59.40	

Site 884: The stratigraphic position of calcareous nannofossil datums in the Leg 145 Initial Reports for Site 884 [*Rea et al.*, 1993] (page 231) were used to create this age model. As depth intervals were listed in top and bottoms depths, the numerical age from *Gradstein et al.* [2004] were applied to the mean depth of the datum from *Rea et al.* [1993]. *Gradstein et al.* [2004] does not assign an age for the last occurrence (LO) of *Discoaster saipanensis*, however the age of LO of *Discoaster barbadiensis* from *Gradstein et al.* [2004] was used for the LO of *Discoaster saipanensis*, as they have the same extinction boundary, identified at Site 884. See Table 7 for datum information.

Table 7. Datums for Site 884 age model.

Site 884				
Biomarker Datum *Rea et al.* [1993]	T Depth (mbsf)	B Depth (mbsf)	Mean Depth (mbsf)	Age (Ma) *Gradstein et al.* [2004]
LO *Ericsonia formosa*	680.60	681.10	680.85	33.00
LO *Discoaster saipanensis*	690.20	699.80	695.00	34.40
FO *Isthmolithus recurvus*	757.70	767.40	762.55	36.20

Site 1208: Calcareous nannofossil datums in the Leg 198 Initial Reports for Site 1208 [*Bralower et al.*, 2002] (Figure 17 and Table 3) were assigned numeric ages from the *Gradstein et al.* [2004] timescale. LO *Discoaster barbadiensis*, LO *Chiasmolithus grandis* and first occurrence (FO) *Reticulofenestra umbilicus* were not included as a

hiatus disrupted the stratigraphic sequence of these datums at Site 1208 (not identified in the correct order). See Table 8 for datum information.

Table 8. Datums for Site 1208 age model.

Site 1208		
Biomarker Datum	Depth	Age (Ma)
*Bralower et al. [*2002]	(mbsf)	*Gradstein et al.* [2004]
LO *Reticulofenestra*	321.10	32.40
LO *Tribrachiatus orthostylus*	326.80	51.20
FO *Discoaster lodoensis*	327.30	52.60
FO *Discoaster multiradiatus*	327.60	57.00
FO *Ceratolithoides aculeus*	366.10	79.00

3.3 *Analytical Methods*

Samples were initially placed in a dilute sodium metaphospate solution to dis-aggregate the sediment before being washed through a 63 micron (μm) sieve. Fish teeth and bones (hereafter referred to as fish debris) were then handpicked from the washed samples. In general, ~40-50 pieces of fish debris were picked from each sample depending upon the size and abundance in the sample. Traditionally, the Boyle oxidative/reductive cleaning protocol has been used to remove any oxide coating and residual organic matter from the fish debris prior to dissolution [*Boyle*, 1981; *Boyle and Keigwin*, 1985]. A growing body of work indicates that this time consuming cleaning step is not necessary because the oxides record the same signal as the fish debris [e.g., *Roberts et al.*, 2010].

To ensure that the oxidative/reductive cleaning protocol is indeed unnecessary, particularly for samples of Paleogene age, and that the signal is the same without the cleaning protocol, I compared a subset of "cleaned" versus "un-cleaned" fish debris (identified as "C" and "UC" respectfully). I analyzed two splits from at least two samples at each site (one that underwent the rigorous Boyle oxidative/reductive cleaning step (C) and one that underwent two rinses in ethanol and two rinses in ultrapure (Milli-Q) water (UC). After verifying that the Boyle cleaning was unnecessary (see Section 4

below) I processed the remaining samples with ethanol and Milli-Q rinses to remove any detrital material.

After removing the detrital material, the fish debris was then dissolved in 2 N HNO_3 before being processed through RE Spec cation exchange chemistry to isolate the REE, followed by methyllactic acid chemistry to chromatographically separate Nd from the rest of the REE. Aqua regia was used to purge the methyllactic acid after the chemistry was completed. Finally, 2 N HCl was added to each dried sample to facilitate loading onto a double rhenium (Re) filament. The entire analytical procedure is described in detail in Appendix A.

All samples were analyzed as Nd+ using the Thermo Triton thermal ionization mass spectrometer (TIMS). Replicate samples, at least two at each site, were analyzed to verify that the Nd values are reproducible (eg., 1-5, 18-20 and 1-5, 18-20 R). Based on replicate analyses of the JNdi standard (0.5121035) the external reproducibility is 6 ppm (1σ). The typical lab blank is 20 pg and is considered negligible.

A representative set of samples was powdered for detrital silicate analysis. The detrital silicate fraction was isolated from carbonate, biogenic apatite, organic carbon, the oxide/hydroxide coatings, and biogenic silica using chemical extraction methods [e.g., *Gutjahr et al.*, 2007]. After extraction, the detrital silicate was digested in HF-HNO_3 and HCl before undergoing the RE Spec cation exchange chemistry and methyllactic acid chemistry to isolate the Nd. The detrital silicate analytical procedure is described in detail in Appendix A.

$\varepsilon_{Nd}(t)$ values were calculated using the numerical ages determined with the age models detailed above. For fish debris, I applied a typical $^{147}Sm/^{144}Nd$ value of 0.13 after *Thomas et al.* [2008]. A $^{147}Sm/^{144}Nd$ value of 0.109 was used in determination of the silicate $\varepsilon_{Nd}(t)$ values based on upper crustal average concentrations of Sm and Nd [*Taylor*

and McLennan, 1995], and a $^{147}Sm/^{144}Nd$ value of 0.115 was used in oxide fraction $\varepsilon_{Nd}(t)$ values based on average Fe-Mn crust values after *Ling et al.* [1997].

4. RESULTS

4.1 *Site 192*

The $\varepsilon_{Nd}(t)$ values recorded by the uncleaned sample range from +2.21 to -3.93 throughout the study interval (Figure 4; Appendix B). Values increase from -1.85 at 1023.02 mbsf (62.41 Ma) to +2.21 at 1020.42 mbsf (54.22 Ma) and then generally decrease from -2.5 to -3.5 over the interval 985.02 to 942.52 mbsf (39.24 to 32.62 Ma).

Comparison of the Nd isotopic values of cleaned samples with the respective uncleaned values indicates similar values (Figure 4; Appendix B): the cleaned fraction from sample 1-1, 52-55 had an $\varepsilon_{Nd}(t)$ value of -3.54 while the uncleaned fraction was -3.59, and the cleaned fraction from sample 2-1, 66-68 had an $\varepsilon_{Nd}(t)$ value of -3.13 while the uncleaned fraction was -3.38.

One analysis of the oxide fraction leached from the bulk sediment recorded an $\varepsilon_{Nd}(t)$ value of +8.00 at 1020.42 mbsf (54.22 Ma).

Three silicate analyses from Site 192 yielded $\varepsilon_{Nd}(t)$ values of +7.95 at 1020.42 mbsf (54.22), to -2.10 at 985.02 mbsf (39.24 Ma), and -2.76 at 945.51 mbsf (33.88 Ma).

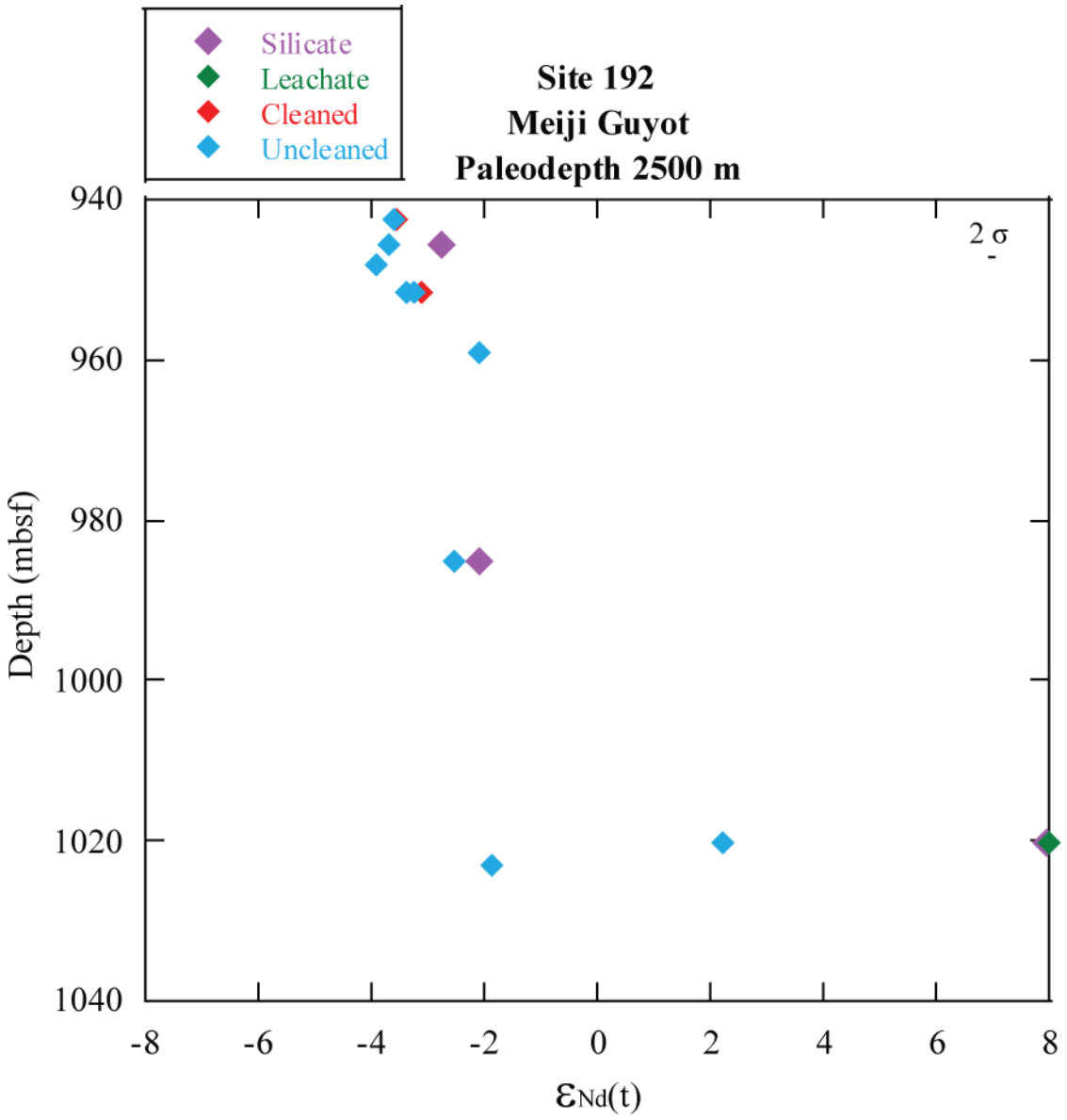

Figure 4. Nd isotopic data generated from Site 192.

4.2 *Site 464*

The $\varepsilon_{Nd}(t)$ values recorded by the uncleaned sample range from 0 to -5.59 throughout the study interval (Figure 5; Appendix B). Values increase from -5.14 at 74.25 mbsf (67.74 Ma) to ~0 to -2 from 62.16 to 49.64 mbsf (61.79 to 54.74 Ma), with the peak of most radiogenic values (0.00) at 58.25 mbsf (59.86 Ma) and then to ~-3 to -4.5 over the interval 48.55 to 42.40 mbsf (54.74 to 13.14 Ma).

Comparison of the Nd isotopic values of cleaned samples with the respective uncleaned values indicates similar values (Figure 5; Appendix B): the cleaned fraction of 6-2, 97-99 had an $\varepsilon_{Nd}(t)$ value of -3.07 while the uncleaned fraction was -3.01, the cleaned fraction of 6-6, 64-66 had an $\varepsilon_{Nd}(t)$ value of -1.33 while the uncleaned fraction was -1.86, the cleaned fraction of 7-1, 50-52 had an $\varepsilon_{Nd}(t)$ value of -1.98 while the uncleaned fraction was -2.13, the cleaned fraction of 7-3, 137-139 had an $\varepsilon_{Nd}(t)$ value of -0.73 while the uncleaned fraction was -0.61 and the cleaned fraction of 9-6, 85-87 had an $\varepsilon_{Nd}(t)$ value of -5.49 while the uncleaned fraction was -5.59. Four additional cleaned values from Site 1208 yielded $\varepsilon_{Nd}(t)$ values of -3.92 for sample 5-3, 50-52, -4.71 for sample 6-1, 57-59, -3.20 for sample 6-5, 44-46 and -1.69 for sample 6-7, 26-28.

Two silicate analyses from Site 464 yielded $\varepsilon_{Nd}(t)$ values of +0.21 at 59.70 mbsf (60.58 Ma) and -5.21 at 42.40 mbsf (33.42 Ma).

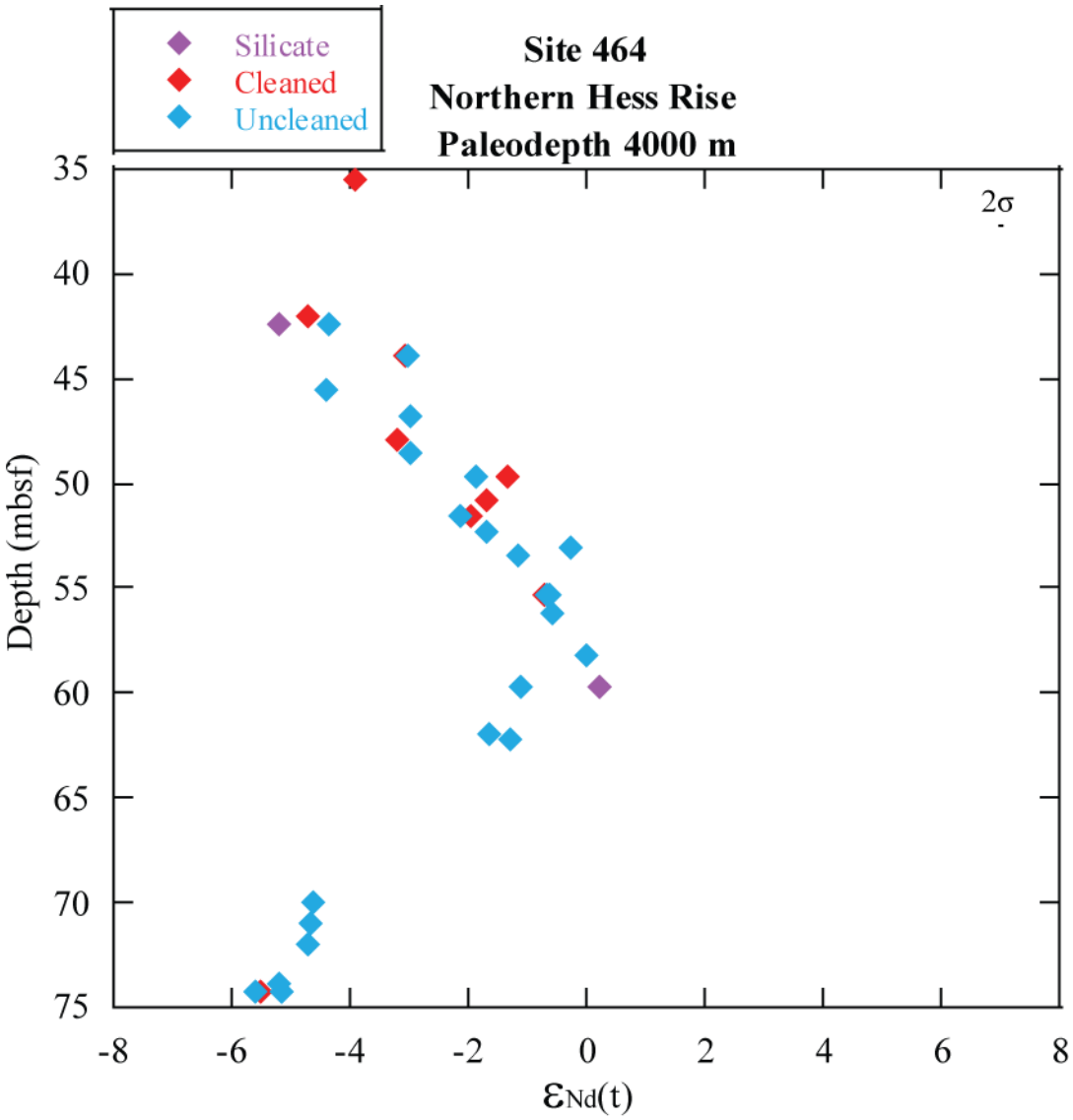

Figure 5. Nd isotopic data generated from Site 464.

4.3 *Site 465*

The $\varepsilon_{Nd}(t)$ values recorded by the uncleaned sample range from -2.79 to -4.29 throughout the study interval (Figure 6; Appendix B). Values increase from -4.29 at 83.28 mbsf (65.99 Ma) to -3.15 to -3.94 from 64.66 to 45.78 mbsf (65.99 to 59.34 Ma) with one notable exception of -4.25 at 79.25 mbsf (65.10 Ma), then increase to values of -2.79 to -2.93 from 36.5 to 11.5 mbsf (57.83 to 55.13 Ma) and then decrease to -3.62 at the top of the study interval (2.22 mbsf, 1.91 Ma).

Comparison of the Nd isotopic values of cleaned samples with the respective uncleaned values indicates similar values (Figure 6; Appendix B): the cleaned fraction from sample 2-1, 122-124 had an $\varepsilon_{Nd}(t)$ value of -3.77 while the uncleaned fraction was -3.62, the cleaned fraction from sample 3-1, 25-27 had an $\varepsilon_{Nd}(t)$ value of -3.90 while the uncleaned fraction was -3.80, the cleaned fraction from sample 3-2, 37-39 had an $\varepsilon_{Nd}(t)$ value of -3.96 while the uncleaned fraction was -3.74 and the cleaned fraction from sample 5-5, 100-102 had an $\varepsilon_{Nd}(t)$ value of -2.89 while the uncleaned fraction was -2.93.

One analysis of the oxide fraction leached from the bulk sediment recorded an $\varepsilon_{Nd}(t)$ value of -3.02 at 42.75 mbsf (58.80 Ma).

Three silicate analyses from Site 465 yielded $\varepsilon_{Nd}(t)$ values of -3.98 at 64.66 mbsf (65.99 Ma), to -3.76 at 58.76 mbsf (64.19 Ma) and -3.07 at 42.75 mbsf (58.80 Ma).

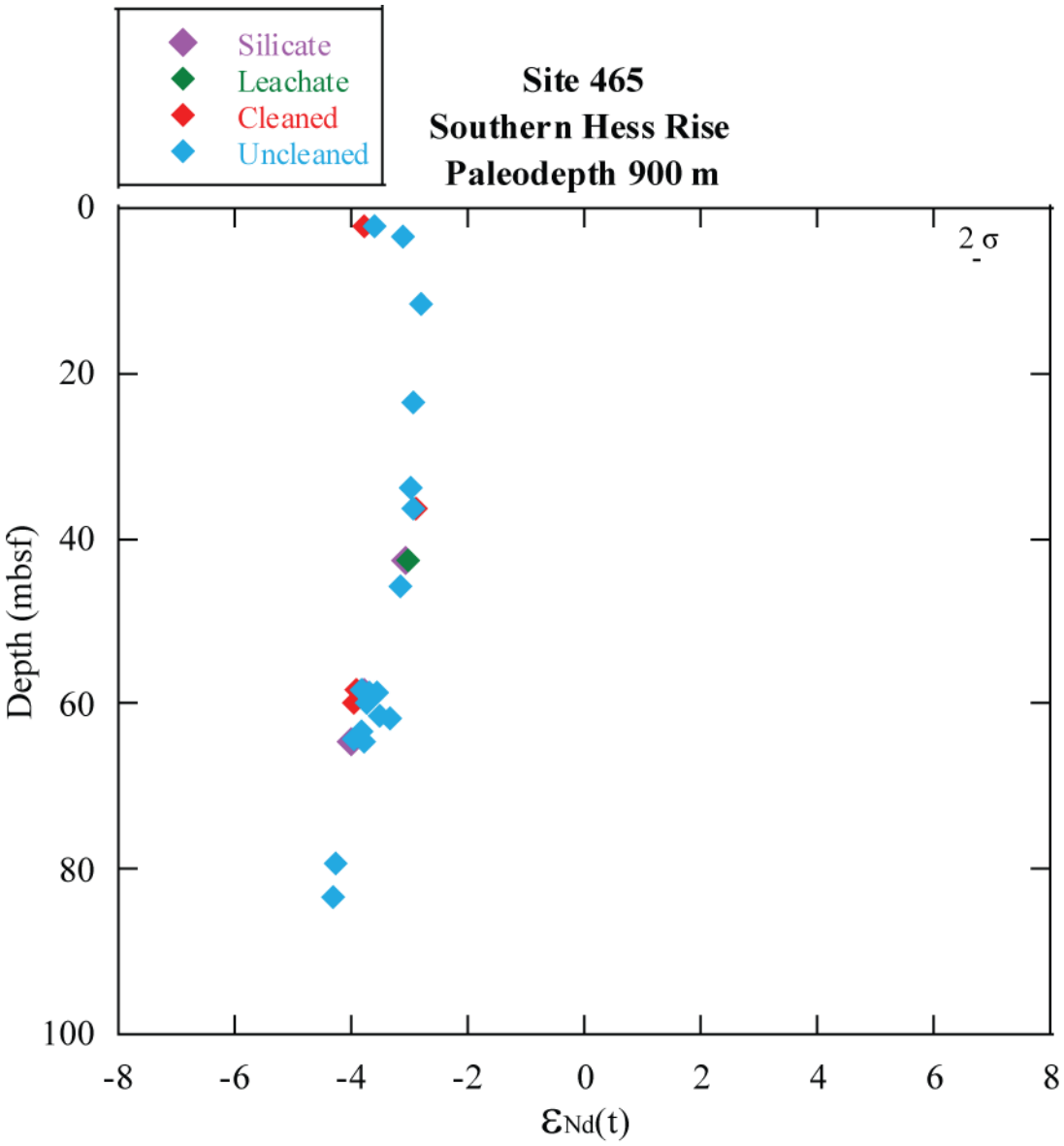

Figure 6. Nd isotopic data generated from Site 465 (Holes 465 * and 465 A).

4.4 *Site 883*

The $\varepsilon_{Nd}(t)$ values recorded by the uncleaned sample range from -2.89 to -3.66 throughout the study interval (Figure 7; Appendix B). Values increase from ~2.1 to +3.7 between 830.25 to 818.70 mbsf (66.49 to 56.59 Ma) and then decrease to ~-1 to -3 from 813.70 to 714.03 (52.56 to 34.73 Ma).

Comparison of the Nd isotopic values of cleaned samples with the respective uncleaned values indicates similar values (Figure 7; Appendix B): the cleaned fraction from sample 83-2, 75-77 had an $\varepsilon_{Nd}(t)$ value of -2.12 while the uncleaned fraction was -1.94 and the cleaned fraction from sample 84-1, 75-77 had an $\varepsilon_{Nd}(t)$ value of -1.90 while the uncleaned fraction was -1.92.

Two analyses of the oxide fraction leached from the bulk sediment recorded an $\varepsilon_{Nd}(t)$ value of +0.40 at 743.35 mbsf (41.57 Ma) and +2.67 at 818.70 mbsf (56.59 Ma).

Three silicate analyses from Site 192 yielded $\varepsilon_{Nd}(t)$ values of +2.31 at 818.70 mbsf (56.59 Ma), to -2.81 at 791.45 mbsf (50.63 Ma) and +2.58 at 743.35 mbsf (41.57 Ma).

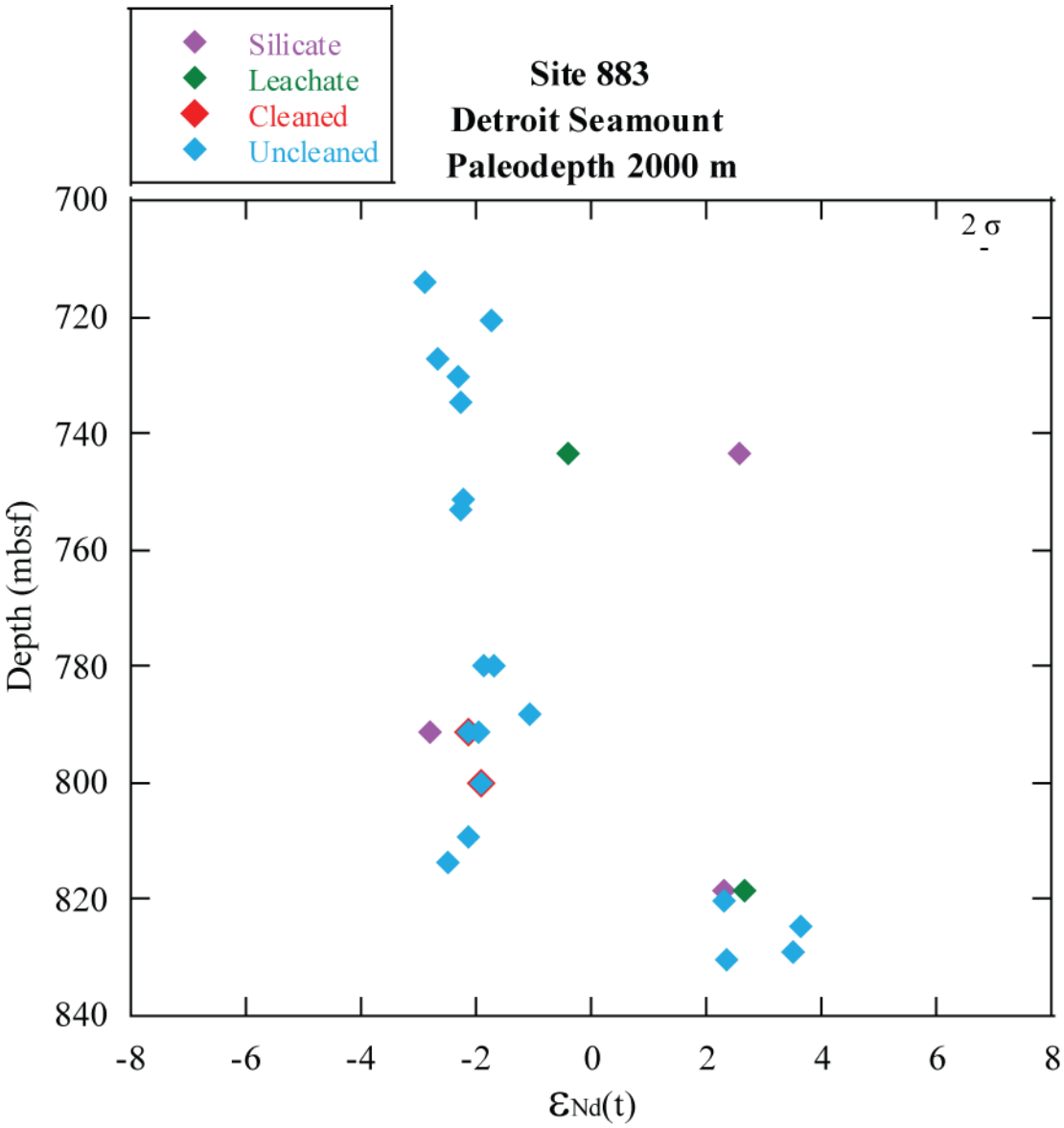

Figure 7. Nd isotopic data generated from Site 883.

4.5 *Site 884*

The $\varepsilon_{Nd}(t)$ values recorded by the uncleaned sample range from -0.61 to -3.76 throughout the study interval (Figure 8; Appendix B). Values increase from -3.71 (average of sample and it's replicate) at 835.53 mbsf (38.14 Ma) to -0.61 at 825.75 mbsf (37.88 Ma) and then from 816.60 to 739.25 mbsf (37.64 to 35.68 Ma) values consistently range from -2.21 to -1.44. At 717.25 mbsf (34.99 Ma) the value is -3.44 and increases to the top of the interval at 687.40 mbsf (33.65 Ma), -1.93.

Comparison of the Nd isotopic values of cleaned samples with the respective uncleaned values indicates similar values (Figure 8; Appendix B): the cleaned fraction from Sample 74-5, 80-83 had an $\varepsilon_{Nd}(t)$ value of -1.68 while the uncleaned fraction was -1.92 and the cleaned fraction from Sample 75-6, 45-47 had an $\varepsilon_{Nd}(t)$ value of -2.39 while the uncleaned fraction was -2.51.

One analysis of the oxide fraction leached from the bulk sediment recorded an $\varepsilon_{Nd}(t)$ value of +5.72 at 731.08 mbsf (35.36 Ma).

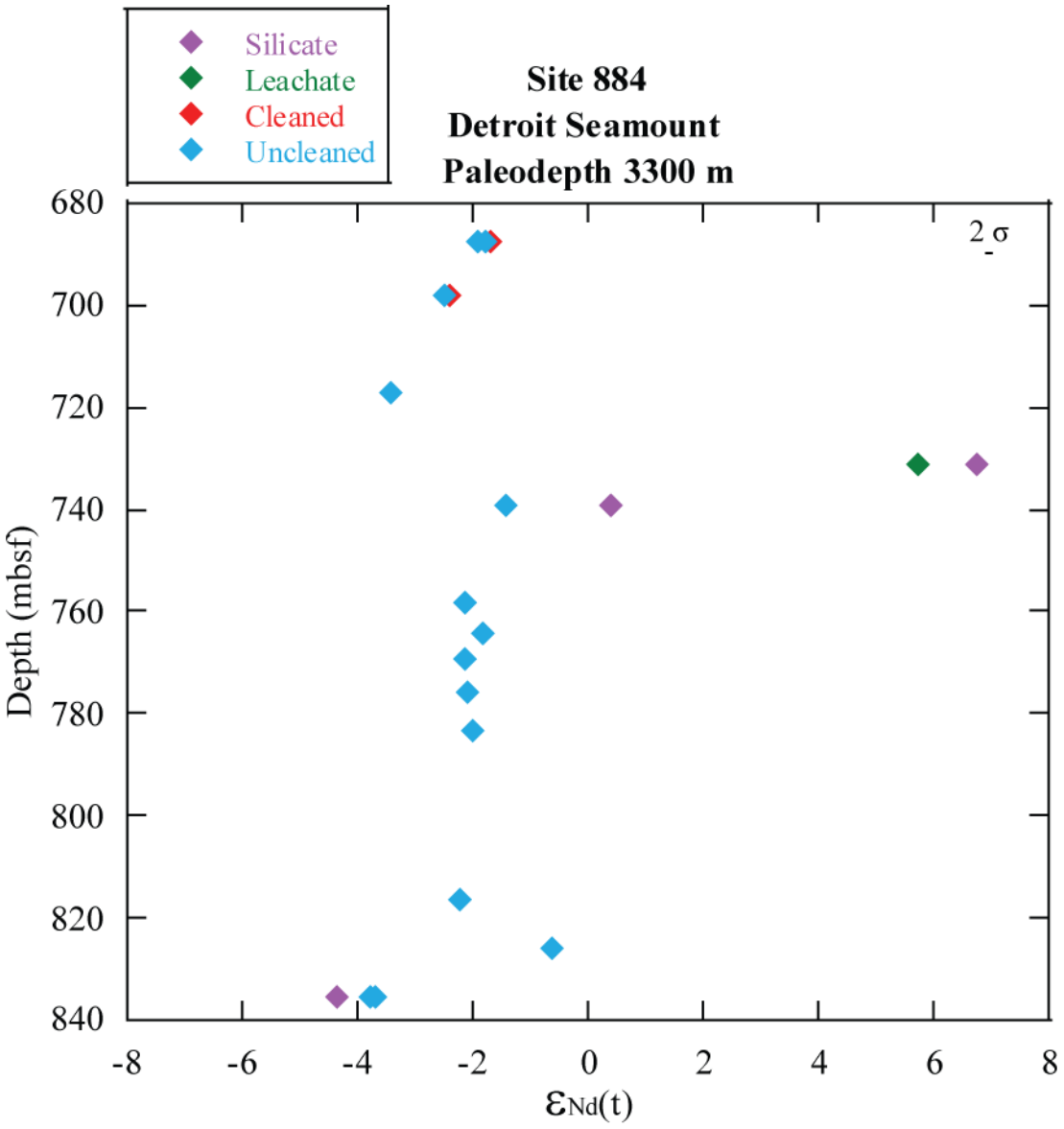

Figure 8. Nd isotopic data generated from Site 884.

4.6 *Site 1208*

The $\varepsilon_{Nd}(t)$ values recorded by the uncleaned sample range from -3.19 to -4.57 throughout the study interval (Figure 9; Appendix B). Values decrease from -3.19 to -3.61 between 327.28 to 326.86 mbsf (52.54 to 51.37 Ma) to -4.35 to -4.57 from 326.68 to 326.43 (50.58 to 49.77 Ma).

Comparison of the Nd isotopic values of cleaned samples with the respective uncleaned values indicates similar values (Figure 9; Appendix B): the cleaned fraction from sample 36-2, 15-17 had an $\varepsilon_{Nd}(t)$ value of -4.47 while the uncleaned fraction was -4.57 and the cleaned fraction from sample 36-2, 28-30 had an $\varepsilon_{Nd}(t)$ value of -4.50 while the uncleaned fraction was -4.35. Six additional cleaned values from Site 1208 yielded $\varepsilon_{Nd}(t)$ values of -4.13 at 375.00 mbsf (84.09 Ma) to -3.75 at 327.61 mbsf (57.01 Ma), with the most non-radiogenic value of -4.34 at 365.30 mbsf (78.54).

Three silicate analyses from Site 1208 yielded $\varepsilon_{Nd}(t)$ values of -3.70 at 326.95 mbsf (51.62 Ma), to -4.32 at 326.68 mbsf (50.58 Ma) and values of -6.55 at 326.43 mbsf (49.77 Ma).

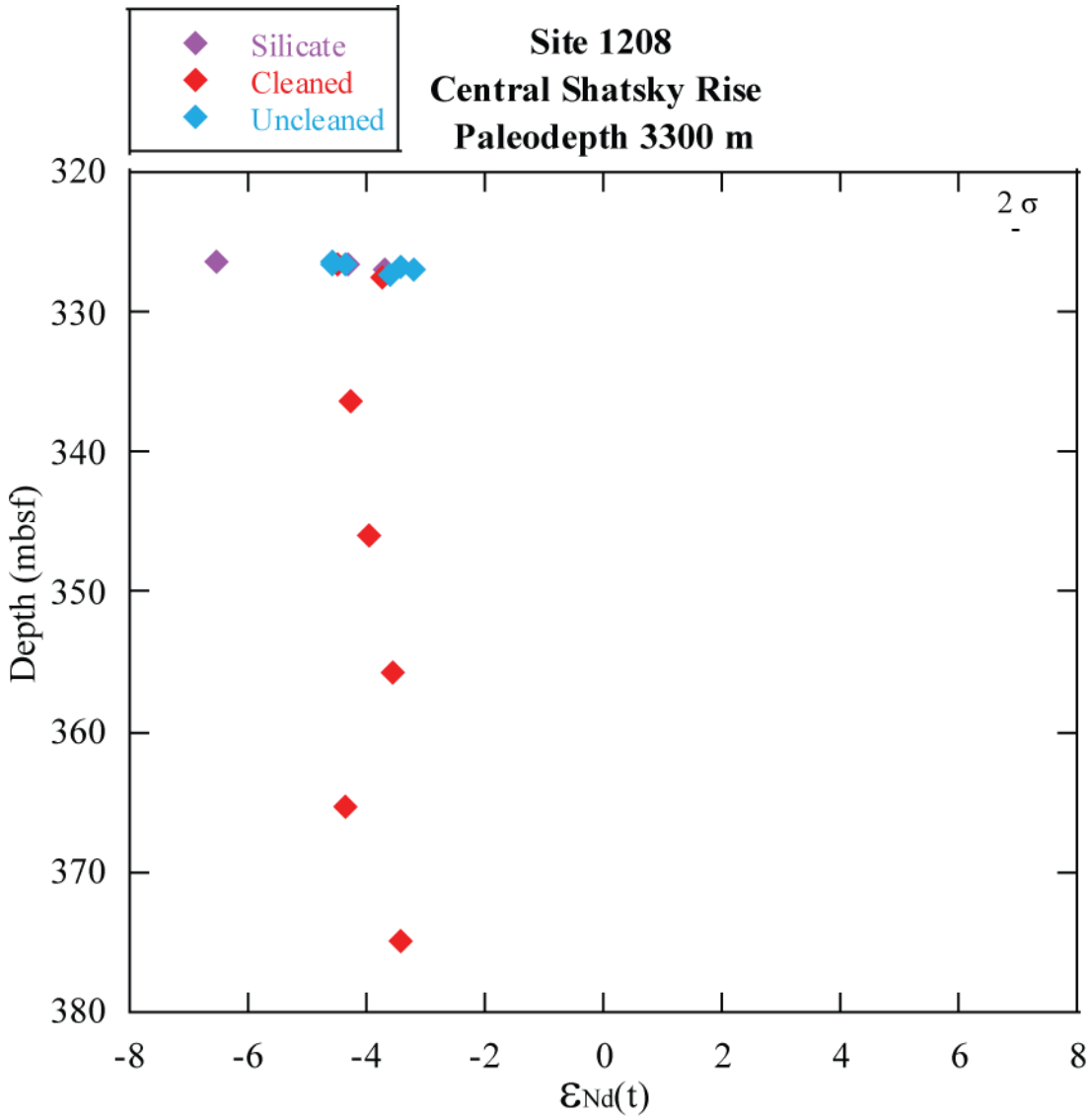

Figure 9. Nd isotopic data generated from Site 1208.

As fish debris was scarce in a few samples the oxide leachate was analyzed. The leachate value should record the same value as the fish debris, the seawater signal. However, leachate values from this study are very close to silicate values. Based on these results we conclude that the leaching protocol was too strong and silicates were leached. Thus, the seawater signal recorded that should be recorded by the leachate has been contaminated.

5. DISCUSSION

5.1 *Assessment of Cleaning Protocol*

Traditionally, the preparation of fish teeth and debris for Nd isotopic analysis included the rigorous "Boyle" oxidative/reductive cleaning protocol [*Boyle*, 1981; *Boyle and Keigwin*, 1985] which removed any potential REE contribution from the biogenic apatite, other than that bound within the apatite lattice itself. Recent studies indicate that the Fe-Mn oxides that are found ubiquitously in oxic waters precipitate at the seafloor [*Roberts et al.*, 2010]. Thus the Nd isotopic composition recorded by the oxide minerals should be identical to that preserved in contemporaneous fish debris. To test this relationship we compared Nd isotopic values obtained from uncleaned (oxides not removed) fish debris to those from cleaned (oxides removed) fish debris. The cleaned and uncleaned fish debris samples indeed record the same isotopic composition (Figure 10). The difference between $\varepsilon_{Nd}(t)$ values for paired cleaned and uncleaned samples ranges from 0.03 to 0.53 epsilon units, with an average difference of 0.15. In addition to the small difference between the paired cleaned and uncleaned fish debris samples, there was no systematic offset between the two (i.e., cleaned values were not consistently higher or lower than the uncleaned values). The average difference between cleaned and uncleaned splits (0.15 epsilon units) is comparable to the external analytical precision (6 ppm or ~0.12 epsilon units, 1σ), and to replicate analyses of similarly prepared samples (Appendix B).

Based on these results we conclude that "cleaned" and "uncleaned" fish debris record the same Nd isotope composition and include both in the reconstruction of water mass composition.

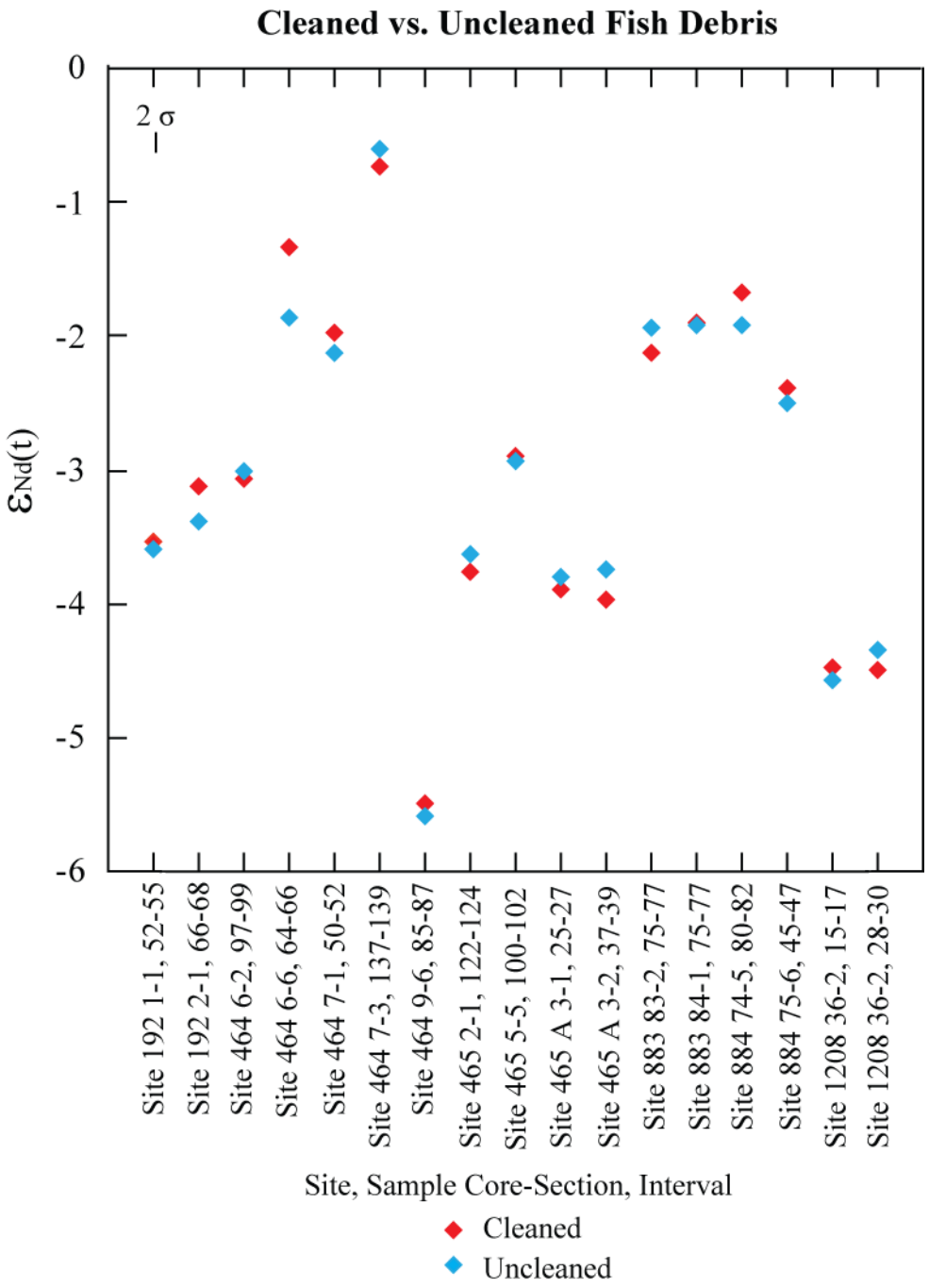

Figure 10. Nd isotopic composition of cleaned vs. uncleaned fish debris.

5.2 *Sources of Detrital Silicates to the North Pacific*

The range of $\varepsilon_{Nd}(t)$ values of the extracted detrital silicates (-6.6 to +7.9; Figure 11) throughout the ~40 Myr study interval suggests mixing among several sources. These sources include unradiogenic eolian dust, radiogenic volcanic ash and radiogenic volcanogenic sediments derived from the weathering and erosion of subaerially exposed portions of seamounts/large igneous provinces and arc terranes. Volcanogenic sediments may have been transported to the sampling locations via wind or hemipelagic processes, or may have been derived locally (particularly in the case of the Emperor Seamount Sites 192, 883 and 884).

The detrital material analyzed in this study is generally radiogenic (Figure 11). This suggests that unradiogenic dust contributions to the study sites were low compared to ash and volcanogenic sediment contributions, and this is consistent with overall low dust accumulation rates during the Paleogene due to a humid greenhouse atmosphere, and fewer and smaller dust source regions [e.g., *Rea*, 1994; *Woodard et al.*, 2011]. The more unradiogenic end member was likely dust supplied from the weathering of older, continental terranes [*Woodard and Thomas*, 2009]. The Nd isotopic composition of eolian dust analyzed from piston core LL44 GPC3 ranges from -10.2 to -6.5 over the interval 70 to 39 Ma [*Pettke et al.*, 2002]. Based on the paleo-latitude of the location as well as the suggestion that the Intertropical Convergence Zone (ITCZ) may have been pushed far to the north of its present location during the Paleogene, eolian material deposited in the North Pacific during this time could have been sourced from North and Central America [*Pettke et al.*, 2002].

The persistence of detrital silicate $\varepsilon_{Nd}(t)$ values greater than 0 throughout most of the study interval suggests a strong contribution of ash/volcanogenic sediments from the circum-North Pacific, particularly at the northernmost sites. Subaerially exposed arc terranes rimming the North Pacific are potential sources of detrital material (ash and current-transported) to the study area. From 75 to 66 Ma an arc to the north of the study

area was narrow, consisting of the Alaska Range-Talkeetna Mountains and Kuskokwim Mountains belts and then from 65 to 56 Ma the arc considerably broadened to include the Yukon-Kanuti belt [*Moll-Stalcup*, 1994]. Volcanism in the interior of Alaska occurred at 40 ± 3Ma and the peak of magmatic activity in the Aleutian arc occurred between 40 and 30 Ma [*Moll-Stalcup*, 1994]. *McCulloch and Perfit* [1981] reported ε_{Nd} values of +6.5 to +9.1 from volcanic and plutonic rocks that span the compositional range of six Aleutian Island arcs (Akutan, Unalaska, Bogoslof, Umnak, Kiska and Segula). To the west of the study area volcanic activity ended at the Lesser Kuril arc during the Late Maastrichtain [*Kronstantinovskaia,* 2001]. While the Achaivayam-Valaginskaya arc was active during the Campanian to Early Paleocene and the Kronotskaya arc was active during the Coniacian to Eocene [*Shapiro*, 1995]. When the Achaivayam-Valaginskaya arc collided with North-east Asia the Koryak-Kamchatka and Central Kamchatka volcanic belts were formed during the Middle Eocene and Oligocene, respectively [*Kronstantinovskaia,* 2001]. Eocene to Oligocene lavas are found along the Izu-Bonin-Mariana system [*Taylor and Nesbitt*, 1995]. Hahajima volcanic rocks, the southernmost island of the Bonin archipelago, provide ε_{Nd} values of +7.1 to +7.7 [*Taylor and Nesbitt*, 1995].

Local contributions of volcanogenic sediments and ash are also potential sources radiogenic detrital material to the sediments at each study site. The Hawaiian-Emperor Seamount chain began forming ~85 Myr. Meiji Guyot (Site 192) lies at the most northern extent of the chain and the tholeiitic basalts here are ~85 Myr while Detroit Seamount (Sites 883 and 884) to the southeast is ~81 Myr [*Regelous et al.*, 2003].

The studied interval from Site 192 consists of chalk and calcareous claystone with no record of discrete ash layers [*Creager et al.*, 1973], however it is likely that disseminated ash existed throughout the section. Portions of the lower Eocene Meiji Guyot section were likely deposited in shallow waters based on graded beds and benthic foraminifera and suggest that portions of the guyot may have been subaerially exposed during the

Cretaceous and early Eocene [*Creager et al.*, 1973]. Thus, some of the detrital silicates at this location may have originated from erosion and weathering of Meiji itself. $\varepsilon_{Nd}(t)$ values of the Meiji tholeiitic basalts range from +7.3 to +8.6 [*Regelous et al.*, 2003]. As the site deepened through the Eocene and into the Oligocene, the likely source of detrital sediments forming the thick clay sequence was weathering of Kamchatka to the west or the Aleutian Ridge to the north [*Creager et al.*, 1973]. This is supported by the trend in detrital values with the deepest silicate value of +7.9 at 1020.42 mbsf (48.21 Ma), much higher than the shallower two silicates (-2.10 at 985.02 mbsf and -2.76 at 945.51 mbsf).

In contrast to Meiji Guyot, Detroit Seamount never experienced subaerial exposure and the sedimentary sequence at Sites 883 and 884 contain abundant ash and altered ash layers [*Rea et al.*, 1993]. Basalt $\varepsilon_{Nd}(t)$ values range from +8.5 to +10.5 [*Regelous et al.*, 2003] and are much higher than the detrital $\varepsilon_{Nd}(t)$ values (Figure 11). Thus the detrital silicates deposited on Detroit Seamount likely reflect ash and transported sediments rather than local weathering contributions.

Northern Hess Rise formed at least ~110 Ma and parts of Hess Rise were above sea level [*Thiede et al.*, 1981], however the lack of carbonate sediments through most of the Site 464 section indicates that this portion of the Northern Hess Rise has remained below the carbonate compensation depth (CCD) since the Late Cretaceous. Abundant zeolites in the Site 464 brown clay sequence suggests altered ash [*Thiede et al.*, 1981]. Site 465 on the Southern Hess Rise consists primarily of nannofossil ooze and foraminifer nannofossil ooze that records normal pelagic carbonate deposition above the CCD [*Thiede et al.*, 1981]. While the southern portion of Hess Rise is shallower than the northern rise, there is no evidence of significant subaerial exposure that could have resulted in local weathering contributions to the detrital sediments. Because the Hess Rise sites do not record significant evidence of volcanism during the Late Cretaceous (as discussed above, regions of the North Pacific were active throughout much of the Cretaceous), *Rea and Harrsch* [1981] suggest the likely source of ash was to the south.

The sediment interval of interest at the Central High of Shatsky Rise, Site 1208, consists of clays likely delivered by bottom currents [*Bralower et al.*, 2002]. While traces of volcanic glass and trace to minor amounts of zeolites [*Bralower et al.*, 2002] suggest that disseminated ash contributed to the detrital fraction throughout the section investigated the detrital $\varepsilon_{Nd}(t)$ values are the lowest of the sites investigated, potentially indicating a greater proportion of unradiogenic eolian dust than at the other sites.

Therefore, due to the two end member sources in this region, silicate values in the study region should lie between ~-10 (purely eolian dust source) to +11 (highest value reported for volcanism in the region-Detroit lavas) depending upon the percentage of each end member input to the region. Silicates from this study record $\varepsilon_{Nd}(t)$ values of -8 to +8 which is within the range suggested by the two end member sources (Figure 11). As the volcanic arcs are the main source of the detrital silicates, $\varepsilon_{Nd}(t)$ values should decrease with increased distance away from the source. This is the pattern observed in the detrital data. The most radiogenic silicate values are found at Sites 192 and 884 (+8.0 and +6.8 respectively), the most northern sites, while the most consistent lower values are found at Sites 1208 and 465, the most southern sites.

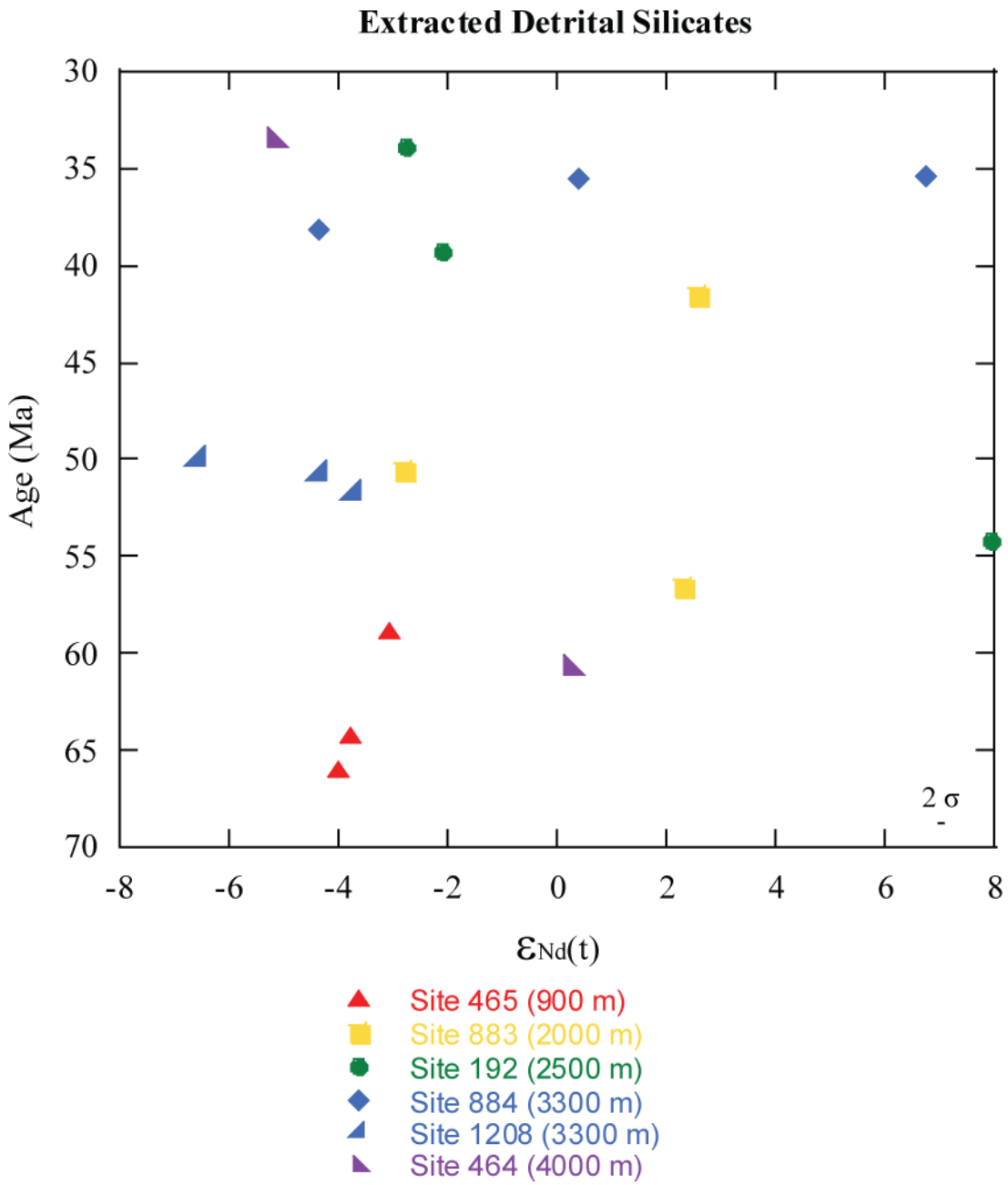

Figure 11. Nd isotopic composition of extracted detrital silicates.

5.3 *Confirmation of Water Mass Formation in the North Pacific*

Fossil fish debris (biogenic apatite) record and retain the Nd isotopic composition of the seawater in which they are deposited [e.g., *Shaw and Wasserburg*, 1985; *Staudigel et al.*, 1985; *Reynard et al.*, 1999; *Martin and Haley*, 2000]. Thus, the fish debris at any given location record the Nd isotopic composition of the intermediate- or deep-water mass that advected into the study location. However, we must consider several processes that may have affected the seawater signal recorded by the fish debris. First, while hydrothermal input of dissolved Nd to the oceans is negligible due to removal by hydrothermal scavenging [*Halliday et al.*, 1992], the prominent peak recorded at Site 883 derives from sediments deposited close to the basement. Thus we must rule out the possibility that very high values at the base of Site 883 reflect the diffusion of hydrothermal Nd from basement into the overlying seawater. Several lines of evidence suggest this was not the case. If hydrothermal Nd was impacting the sediment column above the basement at Site 883 we would expect to see the most influence at the deepest sample. The most radiogenic value is found at 824.55 mbsf, +3.66, not at the deepest sample at 830.25 mbsf, +2.35. In addition, data from ODP Site 1215 suggest that sediments deposited in close proximity to basement are not impacted by hydrothermal Nd contributions. The deepest sample analyzed from Site 1215 which lies on ~58 Ma basement (~70 mbsf) [*Lyle et al*., 2002], shows no indication of hydrothermal Nd from the basement. Here the deepest sample at 55.58 Ma (65.52 mbsf) is -4.15, which is not significantly more radiogenic than any of the other samples in that record spanning 55.58 to 49.30 Ma (-4.49 to -3.40). Thus, it is unlikely that the highly radiogenic values recorded at Site 883 were influenced by additional hydrothermal Nd from the basement. This is also valid for Site 192 where alkali basalts are present at 1044 mbsf [*Creager et al.*, 1973]. The deepest sample from Site 192 is at 1023.02 mbsf yields a value of -1.85 while the most radiogenic seawater value is +2.21 at 1020.42 mbsf. Again, we would expect to see the most influence of hydrothermal Nd at the deepest sample which is not supported by the data thus hydrothermal Nd is not a concern. Furthermore, we are also confident that the unconformity at Site 192 spanning the Paleocene and Early Eocene [*Creager et*

al., 1973] does not affect the sea water composition record. This unconformity only affects the discrepancies in the timing of the peak recorded at Site 192 compared to Sites 464 and 883 due to the stratigraphic resolution and lack of precise age control.

Another factor to consider is that a growing body of work indicates that the water mass Nd isotopic signal may also be overprinted by boundary scavenging in some depositional settings [e.g., *Lacan and Jeandel*, 2005b; *Murphy and Thomas*, 2010]. Therefore, before we can interpret the new fish debris Nd isotope records, we must determine if there was any significant overprinting of the water mass signal that may affect interpretation of the seawater records. Boundary scavenging occurs in deposition settings characterized by high productivity which allows for the local surface water Nd to be transported to the seafloor. As the sites included in this study are far from ancient coastlines in regions of low productivity this is was likely not occurring as the results further suggest.

One way to assess the potential contribution of boundary scavenging at a given location is to analyze the detrital component of the sediment from which the fish debris was extracted. For locations relatively close to land or a subaerially exposed terrane, the detrital component likely reflects the composition of local/regional weathering inputs delivered to the surface waters at the study site. However, the Nd isotopic composition of fluvially-derived detrital sediments is the same as the associated dissolved inputs delivered to the oceanic surface waters [*Goldstein and Jacobsen*, 1987; 1988]. Thus we can assess boundary scavenging by comparing the local detrital composition to that recorded by the fish debris because the composition of the scavenged and released dissolved Nd from local surface waters is the same as the detrital fraction at that location [e.g., *Murphy and Thomas*, 2011].

The impact of boundary scavenging is most profound at productive marginal locations characterized by high fluxes of particles to the seafloor. This is particularly evident in

regions relatively distal to locations of water mass formation. However, the sites investigated here were located far from ancient coastlines. Such locations far from shorelines are typically characterized by low productivity, hence low rates of particle sinking and low potential for transfer of surface water Nd to the seafloor. The fact that there is no systematic offset between the detrital silicate and the fish debris composition (i.e., detrital values were not consistently higher or lower, nor offset by a consistent magnitude, than the fish debris values - Figure 12), also suggests that the water mass composition as recorded by the fish debris was not systematically or significantly overprinted. Thus we rule out the influence of boundary scavenging on the overall trends and values of fish debris Nd at these sites.

Comparison of the detrital silicate and fish debris data indicates a geographic trend in the relative similarity between the two fractions. The southernmost sites investigated generally demonstrate a smaller difference between the detrital and fish debris Nd isotope values, while the more northerly Emperor Seamount sites generally show greater separation between detrital and fish debris values. At Site 465 the difference between paired detrital silicate and fish debris samples is ~0.20 epsilon units. The difference between the Nd isotopic composition of the detrital silicate and fish debris fractions at Sites 464 and 1208 is greater than Site 465. The difference at Site 464 ranges from 0.8 to 1.3 epsilon units, and at Site 1208 from 0.03 to 2 epsilon units. Zeolites are present at both Site 464 and 1208, thus suggesting altered volcanic material could explain the minor separation between the detrital silicate and fish debris values. At Site 192 the range between $\varepsilon_{Nd}(t)$ values for paired detrital silicate and fish debris samples is 0.4 to 5.7 epsilon units, at Site 883 the range is 0.9 (although there is no paired fish debris values for the detrital values of +2.58 and +2.31 where the difference is expected to be great) and at Site 884 the range is 0.6 to 1.8 (although there is no paired fish debris value for the detrital value of +6.76 where the difference is expected to be great).

The geographic trends in detrital silicates vs. fish debris composition, as well as the observation that the most radiogenic detrital values from all sites included in this study occurred at the Emperor Seamount sites, supports the hypothesis that the North Pacific was a location of deep-water convection during the early Paleogene. The overall similarity of detrital and fish debris values at Sites 465 and 1208 likely reflects a stronger influence of more unradiogenic water from the south [e.g., *Thomas,* 2004] and potentially a stronger unradiogenic eolian dust contribution at the southern sites. So why do the more northerly and presumably more proximal Emperor Seamount sites demonstrate greater separation of detrital and fish debris Nd isotopic values? This likely relates to differences in local volcanism and detrital inputs between the Emperor Seamounts and Hess/Shatsky Rises. Meiji Guyot likely supplied local ash/weathering inputs to the seafloor sediments as discussed in Section 5.2. However this portion of the north-central Pacific was likely not a region of intermediate- or deep-water formation based on paleo-geographic constraints (e.g., open ocean location relatively far south) as well as the overall difference between fish debris (dissolved Nd in the water mass) and detrital silicate Nd isotope values. In the case of Detroit Seamount sediments, the detrital fraction was likely not sourced from the seamount itself. Which is supported by the decoupling between the seawater and the detrital composition suggests a different source for both. *Rea and Harrsch* [1981] suggest the likely source of ash was to the south of Hess Rise. While the seawater values were sourced from fluvial inputs to the surface waters of the deep-water convection region. Thus, regardless of the proximity to the presumed location of water mass formation, we would expect some decoupling between detrital and seawater Nd isotopic values if the sources of each fraction were different and had distinct isotopic signatures.

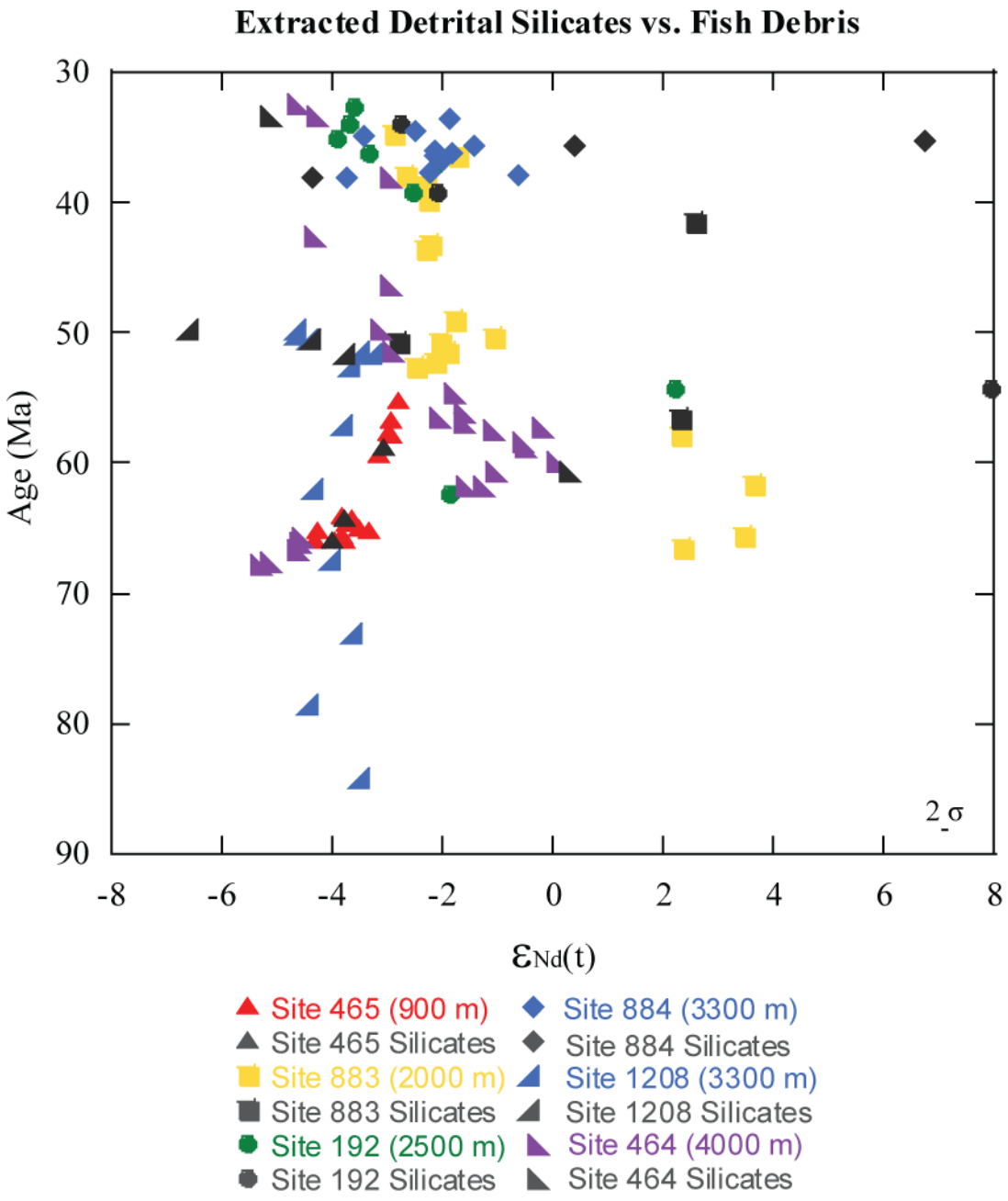

Figure 12. Nd isotopic composition of extracted detrital silicates vs. fish debris.

5.4 *Evolution of North Pacific MOC*

The new fish debris Nd isotope data confirms water mass formation in the North Pacific, but also constrains the timing and influence of the North Pacific deep-water mass. As discussed above, evidence for convection in the North Pacific derives from the combination of fish debris and detrital isotope data, and these data support water mass formation in the North Pacific. Here we discuss the regional influence of the North Pacific deep-water mass based on the Nd isotope values recorded at each site as well as the geographic trends observed within the new and existing data (Figure 13).

The most significant feature in the combined data set is the broadly coincident trends at Sites 192, 464 and 883, where the peak in North Pacific production is recorded Figure 13). Site 192 fish debris Nd isotopic values increase from -1.85 (62.41 Ma), peaking at +2.21 (54.22 Ma), while those at Site 464 increase from -5.37 (67.74 Ma) to +0.21 (60.58 Ma), and Site 883 increase from +2.35 (66.49 Ma) to +3.49 (65.47 Ma) and peak at +3.66 (61.60 Ma). In fact, peak values from Site 883 are the most radiogenic seawater values reported for any ocean basin during the Mesosoic or Cenozoic. Following the broad peak in seawater values, the Nd isotopic composition at the three sites decreases again. At Sites 464 and 883, seawater values stabilize by ~52Ma, and remain fairly constant throughout the rest of the study interval. Discrepancies in the timing of the peak recorded at Site 192 compared to Sites 464 and 883 are due to stratigraphic resolution and lack of precise age control – Site 192 was spot cored and also contains a significant unconformity spanning the Paleocene and Early Eocene [*Creager et al.*, 1973]. Over the interval spanned by the radiogenic shift recorded at Sites 192, 464 and 883, Site 465 recorded a small increase while Site 1208 seawater Nd isotopic values remained essentially constant. By ~50 Ma, the seawater values for all the sites investigated basically converged to a narrow range of isotopic composition (~-2 to -5).

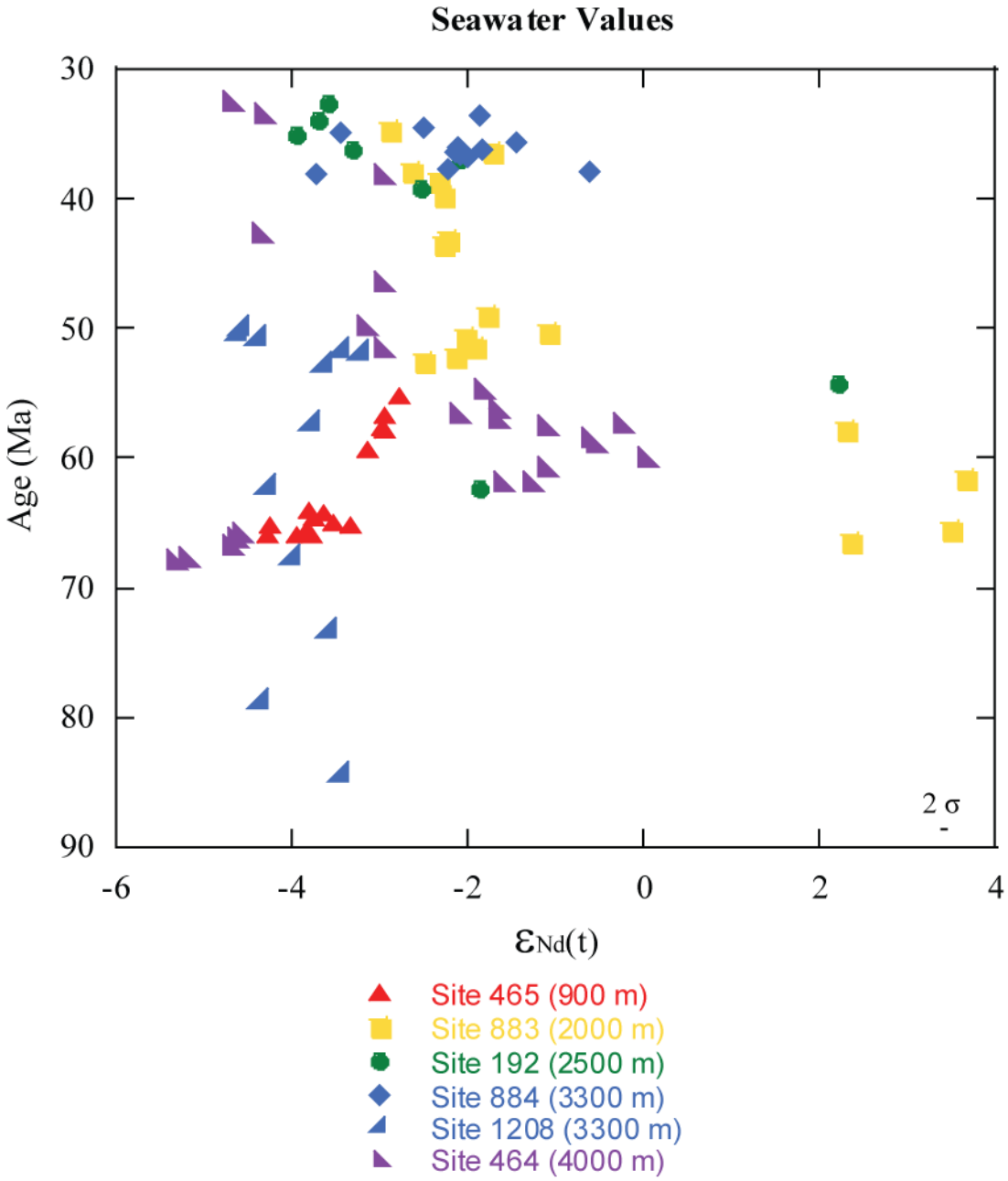

Figure 13. Seawater Nd isotopic records.

The geographic and temporal trends evident in the entire body of Nd isotopic data suggests that deep waters formed in the central North Pacific (Figure 14). The influence of North Pacific deep waters was greatest in the northern sites and weakest in the southern and western sites. Interestingly, Site 464 values are significantly more radiogenic from ~62 to 55 Ma than values from Shatsky Rise (Sites 1208, 1209 and 1211) even though Site 464 on Hess Rise was located at a similar latitude as Shatsky Rise. A possible cause of the isotopic difference is that Site 464 was situated east of the Emperor Seamount chain. The Emperor Seamount chain could have acted as a physical barrier causing the North Pacific deep-water flow to be deflected south along the eastern side of the chain. Thus, the deep Hess Rise Site 464 recorded a more direct influence from the North Pacific than the deep Shatsky Rise Site 1208. The shallower Shatsky Rise Sites 1209 and 1211 (2300 and 2900m water depth, respectively) recorded more radiogenic isotope compositions than Site 1208 suggesting that the Emperor Seamount chain may have restricted water mass flow/exchange at depth, with increased flow at shallower (albeit still deep-water) depths. The Emperor Seamount barrier explains why Site 1208 values are more consistent and do not record a shift like shallower Shatsky Rise Sites 1209 and 1211 record.

Another interesting feature in the overall data set is that Southern Hess Rise Site 465 only records a ~2 epsilon increase in water mass composition during the prominent peak in Nd isotopic values recorded at Sites 192, 464 and 883. This increase is similar to that recorded by Shatsky Rise Sites 1209 and 1211. Site 465 (~900 m water depth) is significantly shallower than Site 1209 and 1211, yet the similar values and trends recorded by the sites suggests a common water mass. The simplest explanation for the data is that convection in the North Pacific produced a dense water mass that influenced the deeper sites in this study more than the shallower sites.

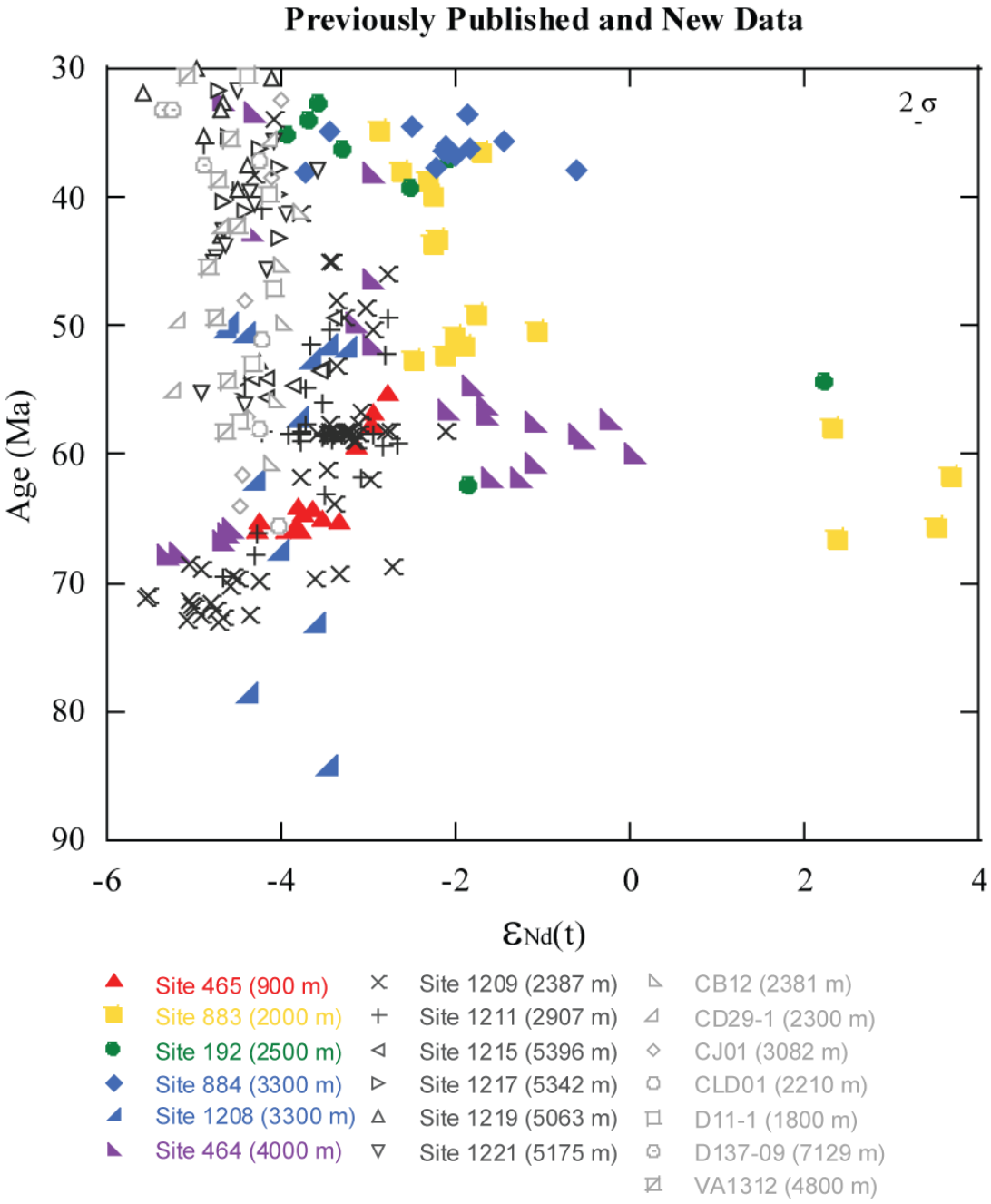

Figure 14. Previously published and newly measured Nd isotopic data. Drill sites (dark grey) and Fe-Mn crusts (light grey) plotted with newly measured data from drill sites (color). Previously measured fish debris and Fe-Mn crust Nd isotope data from *van de Flierdt et al.* [2004]; *Ling et al.* [1997 and 2005]; *Thomas* [2004]; *Thomas et al.* [2008]. Previous drill site paleodepths from *Thomas et al.* [2008] and Fe-Mn crust depths are modern water depths from *Ling et al.* [1997 and 2005] and *van de Flierdt et al.* [2004].

Convection of deep waters in the central North Pacific intensified ~67 Ma and that production began to wane beginning ~60 Ma, based on the trends in the Site 464 and 883 records. By ~52 Ma the influence of North Pacific deep waters had diminished to near "background" levels at the deep-water sites. However, the water mass composition at the shallower Sites 1209 and 1211 remains relatively radiogenic until ~45Ma [*Thomas*, 2004]. The Site 465 sedimentary section contains a hiatus extending to the Pliocene, and hence cannot be used to corroborate the Shatsky Rise trends. Based on the available data, convection in the North Pacific continued until ~45Ma but was not sufficiently intense or the waters were not sufficiently dense to impact the deeper sites.

The new data suggest a pattern of circulation schematically illustrated in Figure 15. As deep water was forming in the North Pacific from ~67 to 45 Ma the radiogenic ε_{Nd} values during this time are sourced from the fluvial input of radiogenic dissolved Nd from the volcanic material rimming the North Pacific. The surface water Nd signal is then exchanged with underlying water masses, intermediate and deep, in regions of deep-water ventilation [*Goldstein and Jacobsen*, 1988; *Elderfield et al.*, 1990; *Halliday et al.*, 1992, *Sholkovitz*, 1993]. Figure 15 A, ~67 Ma, shows deep-water circulation during the peak North Pacific production. Deep waters were forming at ~60° N in the western North Pacific or central North Pacific and then advected south to the study site location. The deep water mass sourced from the Southern Ocean likely influenced the paleoequator and possibly influenced Site 465 and 1208 as ε_{Nd} values are not as radiogenic as at Site 192, 883 and 464. Furthermore, convection in the North Pacific likely produced a dense water mass that influenced the deeper sites more than the shallower sites. Figure 15 B shows deep-water circulation once conditions returned to "background" after ~45Ma, after North Pacific deep-water formation ceased. After ~45 Ma the North Pacific was dominated by Southern Ocean waters advecting north, similar to the modern North Pacific circulation. The initial, less radiogenic AABW signature was overprinted by particle scavenging and exchange with radiogenic inputs along the deep water path. This is supported by ε_{Nd} values of ~-2 to -5 after ~50 Ma, values were

radiogenic but not as radiogenic as during North Pacific deep water formation due to the Southern Ocean water mass dominance.

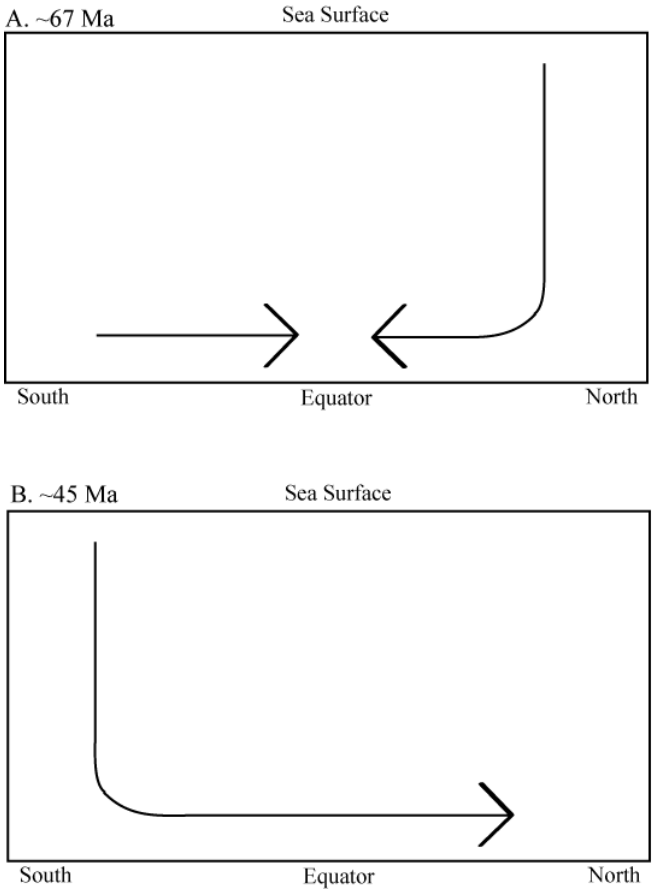

Figure 15. Deep water circulation.

Comparison of the new Nd isotopic records from the North Pacific to the global record of benthic foraminiferal $\delta^{18}O$ values [*Zachos et al.*, 2008] provides some constraint on the relationship between global climate and the evolution of Pacific MOC. The onset of significant convection in the North Pacific coincided with overall Late Cretaceous and Early Paleocene warming, similar to the findings of *Thomas* [2004]. Global warming either altered sea surface hydrology in the North Pacific or in a presumed Southern

Ocean source region, rendering waters in the North Pacific sufficiently dense to convect. All sediment north of Site 192 that would have recorded a change in SSTs, and thus a potential change in sea surface hydrography, has been subducted. The new data present a different climate/MOC relationship than that suggested by *Thomas* [2004]. The timing of the cessation of major, deep convection in the North Pacific occurred much earlier than the timing, ~45 Ma, obtained from shallower Shatsky Rise sites [*Thomas,* 2004]. By ~52 Ma the influence of North Pacific water-mass had diminished to near "background" levels at the deep-water sites which corresponds with the maximum warming of deep-sea temperatures [*Zachos et al.*, 2008]. Thus, suggesting that a deep-sea temperature threshold may have been reached causing North Pacific convection to begin waning at deeper sites, but remaining present at shallower sites until cooling occurred causing complete termination of North Pacific convection.

6. CONCLUSIONS

1. Cleaned and uncleaned fish debris record the same Nd isotope composition. The average difference between the splits (0.15 epsilon units) is comparable to the external analytical precision (6ppm or ~0.12 epsilon units, 1σ), and to replicate analyses of similarly prepared samples.
2. The detrital sediments analyzed in this study are generally radiogenic, thus unradiogenic dust contributions to the study sites were low compared to ash and volcanogenic sediment contributions. Volcanogenic sediments may have been transported to the study region via wind or hemipelagic processes sourced from the circum-North Pacific, or derived locally from the Emperor Seamount.
3. No systematic offset between the detrital silicate and the fish debris composition suggests that the water mass composition recorded by the fish debris was not systematically or significantly overprinted.
4. The geographic trends in detrital silicate vs. fish debris composition, greater separation at the more northerly Emperor Seamount sites, and that the most radiogenic detrital values occur at the Emperor Seamount sites, supports North Pacific deep-water convection during the early Paleogene.
5. The geographic and temporal trends evident in the entire body of Nd isotopic data suggests that deep waters formed in the central North Pacific from ~67 to 45 Ma.
6. The most significant feature in the combined data set is the broadly coincident trends at Sites 192, 464 and 883, where the peak in North Pacific production is recorded.
7. The Emperor Seamount chain likely acted as a physical barrier causing the North Pacific deep-water flow to be deflected south along the eastern side of the chain. Which caused a greater impediment at deeper Shatsky Rise Site 1208 compared to shallower Shatsky Rise Sites 1209 and 1211.
8. Convection in the North Pacific produced a dense water mass that influenced the deeper sites in this study more than the shallower sites until ~52Ma when convection

was not as intense or the waters were not sufficiently dense to impact the deeper sites.

9. Comparison of the ε_{Nd} values to the deep-sea temperatures indicates the timing of the cessation of major, deep convection in the North Pacific occurred much earlier, ~52 Ma, than the timing obtained from shallower Shatsky Rise sites, ~45 Ma. Deep water convection was most intense during the relatively "cool" portion of the Late Cretaceous and Early Paleocene.

REFERENCES

Amakawa, H., D.S. Alibo, and Y. Nozaki (2000), Nd isotopic composition and REE pattern in the surface waters of the eastern Indian Ocean and its adjacent seas, *Geochim. Cosmochim. Acta, 64,* 1715-1727.

Amakawa, H., Y. Nozaki, D.S. Alibo, J. Zhang, K. Fukugawa and H. Nagai (2004), Neodymium isotopic variations in Northwest Pacific waters, *Geochim. Cosmochim. Acta, 68,* 715-727.

Armstrong, H.A., D.G. Pearson and M. Griselin (2001), Thermal effects on rare earth element and strontium isotope chemistry in single conodont elements, *Geochim. Cosmochim. Acta, 65,* 435-441.

Bertram, C.J., and H. Elderfield (1993), The geochemical balance of the rare earth elements and neodymium isotopes in the oceans, *Geochim, Cosmochim. Acta, 57,* 1957-1986.

Boyle, E.A. (1981), Cadmium, zinc, copper, and barium in foraminiferal tests, *Earth Planet. Sci. Lett., 53,* 11-35.

Boyle, E.A., and L.D. Keigwin (1985), Comparison of Atlantic and Pacific paleochemical records for the last 250,000 years: Changes in deep-ocean circulation and chemical inventories, *Earth Planet. Sci. Lett., 76,* 135-150.

Bralower, T.J., I. Premoli Silva, M.J. Malone, M.A. Arthur, K. Averyt, et al. (2002), *Proc. ODP, Init. Repts.,* 198: Ocean Drilling Program, Texas A&M University College Station, TX.

Broecker, W.S., R. Gerard, M. Ewing and B.C. Heezen (1960), Natural radiocarbon in the Atlantic Ocean, *J. Geophys. Res., 65,* 2903-2931.

Broecker, W.S. (1997), Thermohaline circulation, the achilles heel of our climate system: Will man-made CO_2 upset the current balance?, *Science, 278,* 1582-1588.

Creager, J.S., D.W. Scholl, R.E. Boyce, R.J. Echols, T.J. Fullam,et al. (1973), *Proc. DSDP, Init. Repts.,* 19: U.S. Government Printing Office, Washington, DC.

DePaolo, D.J., and G.J. Wasserburg (1976), Nd isotopic variations and petrogenetic models, *Geophys. Res. Lett., 3*, 249-252.

Doyle, P.S., and W.R. Riedel (1981), Ichthyoliths at Site 464 in the Northwest Pacific, Deep Sea Drilling Project Leg 62. In: Thiede, J., T.L. Vallier, C.G. Adelseck Jr., A.

Boersma, P. Cepek, et al. (1981), *Proc. DSDP, Init. Repts.,* 62: Deep Sea Drilling Program,College Station, TX.

Elderfield, H., and M.J. Greaves (1982), The rare earth elements in seawater, *Nature, 296,* 214-219.

Elderfield, H., and R. Pagett (1986), Rare earth elements in ichthyoliths: Variations with redox conditions and depositional environment, *The Science of the Total Environment*, *49,* 175-197.

Elderfield, H., R. Upstill-Goddard and E.R. Sholkolvitz (1990), The rare earth elements in rivers, estuaries, and coastal seas and their significance to the composition of ocean waters, *Geochim. Cosmochim. Acta, 54,* 971-991.

Frakes, L.A., and E.L. Kemp (1972), Influence of continental positions on early Tertiary climates, *Nature, 240,* 97-100.

Goldstein, S.J., and S.B. Jacobsen (1987), The Nd and Sr isotopic systematic of river-water dissolved material: Implications for the sources of Nd and Sr in seawater, *Chem. Geol.: Isotope Geoscience Section, 66,* 245-272.

Goldstein, S.J., and S.B. Jacobsen (1988), Nd and Sr isotopic systematics of river water suspended material: implications for crustal evolution, *Earth Planet. Sci. Lett., 8,* 249-265.

Goldstein, S.L., and S.R. Hemming (2003), Long-lived isotopic tracers in oceanography, paleoceanography, and ice-sheet dynamics. In: Heinrich, D.H. and K.T. Karl (Eds.), *Treatise on Geochemistry,* Pergamon, New York, 453-489.

Goldstein, S.L., D. Zylberberg, K. Pahnke, S.R. Hemming and T. van de Flierdt (2007), Quantifying changes in the global thermohaline circulation: A circum-Antarctic perspective, *US Geological Surveys and The National Acadamies USGS OF- 2007-2047*, Extended Abstract 209.

Gradstein, F., J. Ogg and A. Smith (2004), *A Geologic Time Scale 2004*, Cambridge University Press, Cambridge.

Grandjean, P., H. Cappetta, A. Michard and F. Albarede (1987), The assessment of REE patterns and $^{143}Nd/^{144}Nd$ ratios in fish remains, *Earth Planet. Sci. Lett., 84,* 181-196.

Gutjahr, M., M. Frank, C.H. Stirling, V. Klemm, T. van de Flierdt and A.N. Halliday (2007), Reliable extraction of a deepwater trace metal isotope signal from Fe–Mn oxyhydroxide coatings of marine sediments, *Chem. Geol., 242,* 351-370.

Halliday, A.N., J.P. Davidson, P. Holden, R.M. Owen and A.M. Olivarez (1992), Metalliferous sediments and the scavenging residence time of Nd near hydrothermal vents, *Geophys. Res. Lett., 19,* 761-764.

Jeandel, C. (1993), Concentration and isotopic composition of Nd in the South Atlantic Ocean, *Earth Planet. Sci. Lett., 177,* 581-591.

Jeandel, C., D. Thouron and M. Fieux (1998), Concentrations and isotopic composition of neodymium in the eastern Indian Ocean and Indonesian straits, *Geochim. Cosmochim. Acta, 62,* 2597-2607.

Jones, C.E., A.N. Halliday, D.K. Rea and R.M. Owen (1994), Neodymium isotopic variations in the North Pacific modern silicate sediment and the insignificance of detrital REE contributions to seawater, *Earth Planet. Sci. Lett., 127*, 55-66.

Konstantinovskaia, E.A. (2001), Arc-continent collision and subduction reversal in the Cenozoic evolution of the Northwest Pacific: an example from Kamchatka (NE Russia), *Tectonophysics, 333*, 75-94.

Lacan, F., and C. Jeandel (2001), Tracing Papua New Guinea imprint on the central Equatorial Pacific Ocean using neodymium isotopic compositions and rare earth element patterns, *Earth Planet. Sci. Let., 186,* 497-512.

Lacan, F., and C. Jeandel (2005a), Acquisition of the neodymium isotopic composition of the North Atlantic deep water, *Geochim. Geophys. Geosyst., 6,* Q12008.

Lacan, F., and C. Jeandel (2005b), Neodymium isotopes as a new tool for quantifying exchange fluxes at the continent-ocean interface, *Earth Planet. Sci. Lett., 232*, 245-257.

Lawver, L.A., and L.M. Gahagan (2003), Evolution of Cenozoic seaways in the circum-Antarctic region, *Palaeogeog., Palaeoclimatol., Palaeoecol., 198,* 11-37.

Levitus, S. (1982), Climatological Atlas of the World Ocean, *NOAA Prof. Pap. 13*, U.S. Government Printing Office, Washington, DC.

Ling, H.F., K.W. Burton, R.K. O'Nions, B.S. Kamber, F. von Blanckenburg, A.J. Gibb and J.R. Hein (1997), Evolution of Nd and Pb isotopes in Central Pacific seawater from ferromanganese crusts, *Earth Planet. Sci. Lett., 146,* 1-12.

Lyle, M., P.A. Wilson, T.R. Janecek, J. Backman, W.H. Busch, et al. (2002), *Proc. ODP, Init. Repts.,* 199: Ocean Drilling Program, College Station, TX.

Martin, E.E., and B.A. Haley (2000), Fossil fish teeth as proxies for seawater Sr and Nd, *Geochim. Cosmochim. Acta, 64,* 835-847.

Martin, E.E., and H.D. Scher (2004), Preservation of seawater Sr and Nd isotopes in fossil fish teeth: Bad news and good news, *Earth Planet. Sci. Lett., 220,* 25-39.

Martin, J.E., D. Patrick, A.J. Kihm, F.F. Foit and D.E. Grandstaff (2005), Lithostratigraphy, tephrochronology, and rare earth element geochemistry of fossils at the classical Pleistocene Fossil Lake area, south central Oregon, *J. of Geo., 113,* 139-155.

McCulloch, M.T., and M.R. Perfit (1981), $^{143}Nd/^{144}Nd$, $^{87}Sr/^{86}Sr$ and trace element constrains on the petrogenesis of Aleutian island arc magmas, *Earth Planet. Sci. Lett., 56,* 167-179.

Moll-Stalcup, E.J. (1994), Latest Cretaceous and Cenozoic magmatism in mainland Alaska. In Plafker, G., and H.C. Berg, eds., *The Geology of Alaska*, Geological Society of America, G-1, Geology of North America, Boulder, Colorado, 589-619.

Moran, K., J. Backman, H. Brinkhuis, et al. (2006), The Cenozoic palaeoenvironment of the Arctic Ocean, *Nature, 441,* 601-605.

Murphy, D.P., and D.J. Thomas (2010), The negligible role of intermediate water circulation in stadial-interstadial oxygenation variations along the southern California margin: Evidence from Nd isotopes, *Quat. Sci. Rev., 29*, 2442-2450.

Pearson, P.N., P.W. Ditchfield, J. Singano, K.G. Harcourt-Brown, C.J. Nicholas, R. K. Olsson, N.J. Shackleton and M.A. Hall (2001), Warm tropical sea surface temperatures in the Late Cretaceous and Eocene epochs, *Nature, 413*, 481-487.

Person, A., H. Bocherens, J.-F. Saliège, F. Paris, V. Zeitoun and M. Gérard (1995), Early diagenetic evolution of bone phosphate: An X-Ray-Diffractometry analysis, *J. Arch. Sci., 22,* 211-221.

Pettke,T., A.N. Halliday, and D.K. Rea (2002), Cenozoic evolution of Asian climate and sources of Pacific seawater Pb and Nd derived from eolian dust of sediment core LL44-GPC3, *Paleoceanography, 17*.

Piepgras, D.J., and G.J. Wasserburg (1982), Isotopic composition of neodymium in waters from the Drake Passage, *Science, 217,* 207-214.

Piepgras, D.J., and G.J. Wasserburg (1987), Rare-earth element transport in the western North-Atlantic inferred from Nd isotopic observations, *Geochim. Cosmochim. Acta, 51,* 1257-1271.

Piepgras, D.J., and S.B. Jacobsen (1988), The isotopic composition of neodymium in the North Pacific, *Geochim. Cosmochim. Acta, 52,* 1373-1381.

Rea, D.K., and E.C. Harrsch (1981), Mass-accumulation rates of the non-authigenic inorganic crystalline (eolian) component of deep-sea sediments from Hess Rise, Deep Sea Drilling Project Sites 464, 465, and 466. In: Thiede, J., T.L. Vallier, C.G. Adelseck Jr., A. Boersma, P. Cepek, et al. (1981) *Proc. DSDP, Init. Repts.,* 62: U.S. Government Printing Office, Washington, DC.

Rea, D.K., I.A. Basov, T.R. Janecek, E. Arnold, J.A. Barron, et al. (1993), *Proc. ODP, Init. Repts.,*145: Ocean Drilling Program, Texas A&M University, College Station, TX.

Rea, D.K. (1994), The paleoclimatic record provided by eolian deposition in the deep sea: The geologic history of wind, *Rev. Geophys., 32*, 159-195.

Regelous, M., A.W. Hofmann, W. Abouchami and S.J.G. Galer (2003), Geochemistry of lavas from the Emperor Seamounts, and the geochemical evolution of Hawaiian magmatism from 85 to 42 Ma, *J. Pet., 44*, 113-140.

Reynard, B., C. Lècuyer and P. Grandjean (1999), Crystal-chemical controls on rare-earth element concentrations in fossil biogenic apatites and implications for paleoenvironmental reconstructions, *Chem. Geol. 155,* 233-241.

Roberts, N.L., A.M. Piotrowski, J.F. McManus and L.D. Keigwin (2010), Synchronous deglacial overturning and water mass source changes, *Science, 327,* 75-78.

Saunders, A.D., J.G. Fitton, A.C. Kerr, M.J. Norry and R.W. Kent (1997), The North Atlantic igneous province. In: Mahoney, J.J. and M.F. Coffin (Eds.) Large igneous provinces: Continental, oceanic, and planetary flood volcanism, *AGU Geophys. Monogr., 100*, 45-93, American Geophysical Union, Washington DC.

Shapiro, M.N. (1995), The Upper Cretaceous Achaivayam-Valaginian volcanic arc and kinematics of the North Pacific plates, *Geotectonics, 29*, 52-64.

Shaw, H.F., and G.J. Wasserburg (1985), Sm-Nd in marine carbonates and phosphates, *Geochim. Cosmochim. Acta, 49,* 503-518.

Shimizu, H., K. Tachikawa, A. Masuda and Y. Nozaki (1994), Cerium and neodymium isotope ratios and REE patterns in seawater from the North Pacific Ocean, *Geochim. Cosmochim. Acta, 58,* 323-333.

Sholkovitz, E.R. (1993), The geochemistry of rare earth elements in the Amazon River estuary, *Geochim. Cosmochim. Acta, 58,* 2181-2190.

Sluijs, A., S. Schouten, M. Pagani, et al. (2006), Subtropical Arctic Ocean temperatures during the Palaeocene/Eocene thermal maximum, *Nature, 441,* 610-613.

Staudigel, H., P. Doyle and A. Zindler (1985), Sr and Nd isotope systematics in fish teeth, *Earth Planet. Sci. Lett., 76,* 45-56.

Stott, L.D., J.P. Kennett, N.J. Shackleton and R.M. Corfield (1990), The evolution of Antarctic surface waters during the Paleogene: Inferences from the stable isotopic compositions of planktonic foraminifers, ODP Leg 113. In: Barker, P.F., J.P. Kennett, et al. (1990) *Proc. ODP, Sci. Results,* 113: Ocean Drilling Program, College Station, TX.

Stordal, M.C., and G.J. Wasserburg (1986), Neodymium isotopic study of Baffin Bay water: Sources of REE from very old terranes, *Earth Planet. Sci. Lett., 77,*259-272.

Tachikawa, K., C. Jeandel and M. Roy-Barman (1999), A new approach to the Nd residence time in the ocean: The role of atmospheric inputs, *Earth Planet. Sci. Lett., 170,* 433-446.

Taylor, R.N., and R.W. Nesbitt (1995), Arc volcanism in an extensional regime at the initiation of subduction: A geochemical study of Hahajima, Bonin Islands, Japan. In: Smellie, J.L. (ed.) (1995), *Volcanism Associated with Extension at Consuming Plate Margins, Geol. Soc. Am. Special Paper, 81*, 115-134.

Taylor, S.R., and S.M. McLennan (1995), The geochemical evolution of the continental crust, *Rev. Geophys., 33*, 241-265.

Theyer, F., and S.R. Hammond (1974), Paleomagnetic polarity sequence and radiolarian zones, Brunhes to polarity epoch 20*, *Earth Planet. Sci. Lett., 22,* 307-319.

Thiede, J., T.L. Vallier, C.G. Adelseck Jr., A. Boersma, P. Cepek, et al. (1981), *Proc. DSDP, Init. Repts.,* 62: U.S. Government Printing Office, Washington, DC.

Thomas, D.J. (2004), Evidence for production of North Pacific deep waters during the early Cenozoic greenhouse, *Nature, 430,* 65-68.

Thomas, D.J., and R.K. Via (2007), Neogene evolution of Atlantic thermohaline circulation: Perspective from Walvis Ridge, southeastern Atlantic Ocean, *Paleoceanography, 22*, PA2212.

Thomas, D.J., M. Lyle, T.C. Moore Jr. and D.K. Rea (2008), Paleogene deepwater mass composition of the tropical Pacific and implications for thermohaline circulation in a greenhouse world, *Geochim. Geophys. Geosyst., 9*, Q02002.

Tomczak, M., and J.S. Godfrey (1994), *Regional Oceanography: An Introduction,* Pergamon, London.

van de Flierdt, T., M. Frank, A.N. Halliday, J.R. Hein, B. Hattendorf, D. Günther and P.W. Kubik (2004), Deep and bottom water export from the Southern Ocean to the Pacific over the past 38 million years, *Paleoceanography, 19*, PA1020.

von Blanckenburg, F. (1999), Perspectives: Paleocaenography – Tracing past ocean circulation?, *Science, 286*, 1862-1863.

Woodard, S.C., and D.J. Thomas (2009), Is it eolian dust? Contributions to the fine silicate fraction of deep sea sediments on Shatsky Rise, 58 Ma, *Geochim. Cosmochim. Acta, 73*, Suppl., Abstract A1452.

Woodard, S.C., D.J. Thomas, S. Hovan, U.Röhl and T. Westerhold (2011), Evidence for orbital forcing of dust accumulation during the early Paleogene greenhouse, *Geochim. Geophys. Geosyst., 12*, Q02007.

Wright, J., R.S. Seymour and H.F. Shaw (1984), REE and Nd isotopes in conodont apatite: Variations with geological age and depositional environment, *Spec. Pap. Geol. Soc. Am., 196,* 325-340.

Zachos, J.C., M. Pagani, L. Sloan, E. Thomas and K. Billups (2001), Trends, rhythms, and aberrations in global climate 65 Ma to present, *Science, 292,* 686-693.

Zachos, J.C., G.R. Dickens and R.E. Zeebe (2008), An early Cenozoic perspective on greenhouse warming and carbon-cycle dynamics, *Nature, 451*, 279-283.

Zhang, Y., F. Lacan and C. Jeandel (2008), Dissolved rare earth elements tracing lithogenic inputs over the Kerguelen Plateau (Southern Ocean), *Deep Sea Res., Part II, 55,* 638-652.

APPENDIX A

SAMPLE PROCEDURE

I. Sieving

A dilute sodium metaphospate solution was used to dis-aggregate the sediment before washing through a 63 μm sieve. For those samples that the initial dilute sodium metaphospate solution did not dis-aggregate the sediment mineral oil was used to do so. Mineral oil was added to dried samples and left to soak overnight. The mineral oil was decanted off and hot water was added to the samples. When the hot water was added it pushed the mineral oil out of the pore space within the sample, leaving the sample as fluff. All samples were then washed through a 63 μm sieve. Fish debris was then handpicked from this portion and no debris with a clay coating was included.

II. Cleaning

To ensure that the oxidative/reductive cleaning protocol was indeed unnecessary, a subset of "cleaned" (C) versus "un-cleaned" (UC) fish debris was completed.

The cleaned subset of samples were initially rinsed and sonicated twice with ethanol and then rinsed and sonicated twice with Milli-Q water. The samples were then processed through the oxidative/reductive cleaning protocol. For the oxidative step 200 μL of 0.1 N NaOH and 30% hydrogen peroxide (H_2O_2) was added to each sample and were then placed into a 80˚C hot water bath for ten minutes. The liquid was then aspirated off and the samples were rinsed and sonicated with Milli-Q three times. Next, for the reductive step 100 μl of ammonium hydroxide (NH_4OH), citrate and hydrazine (NH_3NH_3) were added to each sample and placed in the 80˚C hot water bath for thirty minutes. Again, the liquid was aspirated off and the samples were rinsed and sonicated with Milli-Q three times. Finally, an acid leach was completed on each sample that consisted of adding 150 μl of 0.001N HNO_3 to each sample and pipetted it off. Once the

oxidative/reductive cleaning protocol was completed the samples were dissolved in 200 µl of 2N HNO_3.

After verifying that the Boyle cleaning [*Boyle*, 1981; *Boyle and Keigwin*, 1985] was unnecessary the remaining samples were processed in the uncleaned manner with just ethanol and Milli-Q rinses before being dissolved in 200 µl of 2N HNO_3.

III. RE Spec

RE Spec cation exchange chemistry was employed to isolate the REE suite from the bulk sample. RE Spec resin in Milli-Q was loaded into columns, cleaned twice with 3 mL of 0.05 N HNO_3 and then preconditioned with 3 mL of 2 N HNO_3. The samples, already in 200 µl of 2 N HNO_3, were then added to the columns. A series of washes were then added to each column including three 0.1 mL aliquots 2 N HNO_3, two 0.5 mL aliquots of 2 N HNO_3, one 1.0 mL aliquot 2 N HNO_3, and one 1.5 mL aliquot of 2 N HNO_3. Finally, the REE were eluted with 4 mL of warm 0.05 N HNO_3 and then placed on the hot plate to evaporate. At the end of the RE Spec chemistry the samples were dried down as a nitrate and converted to a chlorite prior to the next set of chemistry. To do this, 50 µL of 1 N HCl and 450 µL of Milli-Q were added to each sample for a total of 500 µL of 0.1 N HCl.

IV. Methyllactic Acid Chemistry

Nd was then chromatographically separated from the rest of the REE. BioRad resin in 0.15 M α-HIBA acid was loaded into each column. The resin was set with 200 µL of Milli-Q. The warmed samples, already in 500 µL of 0.1 N HCl, were then loaded into each column. Another 200 µL aliquot of Milli-Q was added to each column to set the sample. Samples were then washed with 10 mL/10.75 mL (two batchs of α-HIBA acid) 0.15 α-HIBA acid, 5.5 mL/5.75 mL of 0.225 α-HIBA acid, and then Nd was eluted with 3.25 mL of 0.225 α-HIBA acid. Samples were then placed on a hotplate to evaporate, with aqua regia to purge any remaining methylatic acid fibrous crystals.

V. TIMS

Finally, 2N HCl was added to each dried sample to load onto a double rhenium (Re) filament. All samples were analyzed as Nd+ using the TIMS.

VI. Leachate and Silicate Samples

The representative set of samples analyzed for the Nd isotopic composition of the detrital silicate fraction were processed as following. To each ~0.05g powdered sample a 50 mL mixture of 52/48 1 M sodium acetate/1 M acetic acid was added and placed on a shaker table for an hour and a half to digest carbonate in the samples. The samples were centrifuged down and the leachate was decanted off. Milli-Q was added to the solid residue, vortexed to allow contact with all the material, and centrifuged down three times. This step was not repeated for any of the samples as there was no reaction occurring after the first decarbonation. Next, 14 mL of 0.02 M hydroxylamine hydrochloride (HH) in 20% acetic acid was added to each sample and again placed on the shaker table for an hour and half. The oxide leachate was decanted off of all samples. For those samples the leachate was going to analyzed (fish debris not abundant in the sample) the leachate was centrifuged down for an hour, poured into a beaker, leaving fines behind, and evaporated off on a hotplate. The remaining solid residue was covered with 0.02 M HH in 20% acetic acid and allowed to soak overnight. After decanting the HH solution the samples were rinsed three times with Milli-Q and dried down. The detrital silicate was then powdered and 0.2 g of the material was weighed out. The samples were then digested in 1 mL concentrated HNO_3 and 3.25 mL HF on the hotplate for several days, until no particles were visible. After being dried down, the samples were then digested in 5 mL concentrated HNO_3 and again allowed to sit on the hotplate for several days until no particles were visible. At this point the leachate and silicate samples then underwent the same RE Spec cation exchange chemistry and methyllactic acid chemistry as completed with the fish debris samples.

APPENDIX B

Nd isotopic data generated in this study. "S" denotes Silicate, "L" denotes Leachate, "C" denotes Cleaned, "UC" denotes Uncleaned and "R" denotes Replicate.

Core-Sec, Int, Type	Depth (mbsf)	143/144	Std Error (abs)	ε_{Nd}	Error	$\varepsilon_{Nd}(t)$	Age (Ma)
Site 192 A							
1-1, 52-55 C	942.52	0.5124427	2.251103E-06	-3.81	0.04	-3.54	32.62
1-1, 52-55	942.52	0.5124398	1.006513E-06	-3.87	0.02	-3.59	32.62
1-3, 51-53 S	945.51	0.5124770	1.444093E-06	-3.14	0.03	-2.76	33.88
1-3, 51-53	945.51	0.5124346	1.534572E-06	-3.97	0.03	-3.68	33.88
1-5, 18-20	948.18	0.5124217	1.964863E-06	-4.22	0.04	-3.93	35.01
1-5, 18-20 R	948.18	0.5124217	1.562724E-06	-4.22	0.03	-3.93	35.01
2-1, 66-68 C	951.66	0.5124622	1.595715E-06	-3.43	0.03	-3.13	36.26
2-1, 66-68	951.66	0.5124493	2.709432E-06	-3.68	0.05	-3.38	36.26
2-1, 66-68 R	951.66	0.5124562	1.879789E-06	-3.55	0.04	-3.24	36.26
2-6, 57-59	959.07	0.5125158	1.193120E-06	-2.38	0.02	-2.08	36.92
3-2, 52-54 S	985.02	0.5125079	9.589225E-07	-2.54	0.02	-2.10	39.24
3-2, 52-54	985.02	0.5124911	2.796151E-06	-2.87	0.05	-2.54	39.24
4-2, 92-94 S	1020.42	0.5130144	5.186006E-06	7.34	0.10	7.95	54.22
4-2, 92-94 L	1020.42	0.5130192	9.266231E-07	7.44	0.02	8.00	54.22
4-2, 92-94	1020.42	0.5127278	4.500798E-06	1.75	0.09	2.21	54.22
4-4, 52-54	1023.02	0.5125165	1.359679E-06	-2.37	0.03	-1.85	62.41
Site 464							
5-3, 50-52 C	35.51	0.5124316	3.100000E-06	-4.03	0.06	-3.92	13.14
6-1, 57-59 C	42.08	0.5123826	1.800000E-06	-4.98	0.04	-4.71	32.48
6-1, 90-92 S	42.40	0.5123517	1.082809E-06	-5.58	0.02	-5.21	33.42
6-1, 90-92	42.40	0.5123996	2.255775E-06	-4.65	0.04	-4.37	33.42
6-2, 97-99 C	43.97	0.5124645	2.288781E-06	-3.38	0.04	-3.07	38.05
6-2, 97-99	43.97	0.5124676	1.681550E-06	-3.32	0.03	-3.01	38.05
6-3, 100-102	45.50	0.5123940	1.799658E-06	-4.76	0.04	-4.40	42.55
6-4, 80-82	46.80	0.5124645	1.481038E-06	-3.39	0.03	-3.00	46.38
6-5, 44-46 C	47.95	0.5124526	3.200000E-06	-3.62	0.06	-3.20	49.76
6-5, 105-107	48.55	0.5124627	1.262694E-06	-3.42	0.02	-2.99	51.53
6-6, 64-66 C	49.64	0.5125463	3.038794E-06	-1.79	0.06	-1.33	54.74
6-6, 64-66	49.64	0.5125193	1.572598E-06	-2.32	0.03	-1.86	54.74
6-7, 26-28 C	50.77	0.5125271	2.300000E-06	-2.16	0.04	-1.69	56.18

Core-Sec, Int, Type	Depth (mbsf)	143/144	Std Error (abs)	ε_{Nd}	Error	$\varepsilon_{Nd}(t)$	Age (Ma)
7-1, 50-52 C	51.50	0.5125125	1.767155E-06	-2.45	0.03	-1.98	56.54
7-1, 50-52	51.50	0.5125044	1.581605E-06	-2.61	0.03	-2.13	56.54
7-1, 125-127	52.25	0.5125262	1.586684E-06	-2.18	0.03	-1.70	56.91
7-2, 60-62	53.10	0.5125988	5.291740E-06	-0.76	0.10	-0.28	57.33
7-2, 100-102	53.50	0.5125544	1.721994E-06	-1.63	0.03	-1.15	57.52
7-3, 137-139 C	55.37	0.5125756	3.604107E-06	-1.22	0.07	-0.73	58.44
7-3, 137-139	55.37	0.5125814	8.006363E-06	-1.10	0.16	-0.61	58.44
7-3, 137-139 R	55.37	0.5125789	3.763650E-06	-1.15	0.07	-0.66	58.44
7-4, 70-72	56.20	0.5125829	2.773767E-06	-1.08	0.05	-0.58	58.85
7-5, 125-127	58.25	0.5126122	3.194823E-06	-0.50	0.06	0.00	59.86
7-6, 120-122 S	59.70	0.5126138	5.197890E-06	-0.47	0.10	0.21	60.58
7-6, 120-122	59.70	0.5125542	1.581869E-06	-1.63	0.03	-1.13	60.58
8-2, 70-72	62.02	0.5125274	1.753841E-06	-2.16	0.03	-1.64	61.72
8-2, 84-86	62.16	0.5125445	1.593132E-06	-1.82	0.03	-1.31	61.79
9-1, 4-6	70.04	0.5123731	5.596361E-07	-5.17	0.01	-4.62	65.67
9-1, 95-97	70.95	0.5123707	1.273097E-06	-5.21	0.02	-4.66	66.11
9-4, 92-94	71.95	0.5123674	1.081635E-06	-5.28	0.02	-4.72	66.61
9-6, 46-48	73.86	0.5123421	1.948303E-06	-5.77	0.04	-5.21	67.55
9-6, 85-87 C	74.25	0.5123276	7.663950E-06	-6.05	0.15	-5.49	67.74
9-6, 85-87	74.25	0.5123223	5.783246E-06	-6.16	0.11	-5.59	67.74
9-6, 85-87 R	74.25	0.5123452	1.455579E-06	-5.71	0.03	-5.14	67.74
Site 465							
2-1, 122-124 C	2.22	0.5124438	1.139200E-05	-3.79	0.22	-3.77	1.91
2-1, 122-124	2.22	0.5124518	2.033023E-06	-3.63	0.04	-3.62	1.91
2-2, 92-94	3.42	0.5124777	1.901269E-06	-3.13	0.04	-3.11	2.59
3-1, 100-102	11.50	0.5124712	2.605133E-06	-3.25	0.05	-2.79	55.13
4-3, 55-57	23.55	0.5124632	3.227790E-06	-3.41	0.06	-2.93	56.77
5-3, 127-129	33.77	0.5124617	1.907070E-06	-3.44	0.04	-2.96	57.61
5-5, 100-102 C	36.50	0.5124648	6.756716E-06	-3.38	0.13	-2.89	57.83
5-5, 100-102	36.50	0.5124628	9.941274E-07	-3.42	0.02	-2.93	57.83
6-3, 75-77 S	42.75	0.5124472	1.451018E-06	-3.72	0.03	-3.07	58.80
6-3, 75-77 L	42.75	0.5124520	6.503761E-07	-3.63	0.01	-3.02	58.80
6-5, 78-80	45.78	0.5124507	2.635476E-06	-3.65	0.05	-3.16	59.34
6-5, 78-80 R	45.78	0.5124512	3.639001E-06	-3.64	0.07	-3.15	59.34
10-2, 75-77	79.25	0.5123919	2.891328E-06	-4.80	0.06	-4.25	65.10
10-5, 83-85	83.28	0.5123897	1.631502E-06	-4.84	0.03	-4.29	65.99

Core,Sec,Int	Depth (mbsf)	143/144	Std Error (abs)	ε_{Nd}	Error	$\varepsilon_{Nd}(t)$	Age (Ma)
Site 465 A							
3-1, 25-27 C	58.25	0.5124108	5.548454E-06	-4.43	0.11	-3.90	64.02
3-1, 25-27	58.25	0.5124159	4.150741E-06	-4.33	0.08	-3.80	64.02
3-1, 76-78 S	58.76	0.5124086	5.812502E-07	-4.48	0.01	-3.76	64.19
3-1, 76-78	58.76	0.5124275	2.022941E-06	-4.11	0.04	-3.57	64.19
3-1, 76-78 R	58.76	0.5124216	2.266895E-06	-4.22	0.04	-3.68	64.19
3-2, 37-39 C	59.87	0.5124072	5.732273E-06	-4.50	0.11	-3.96	64.55
3-2, 37-39	59.87	0.5124187	2.378968E-06	-4.28	0.05	-3.74	64.55
3-3, 35-37	61.35	0.5124292	3.648356E-06	-4.07	0.07	-3.53	65.00
3-3, 68-70	61.68	0.5124388	2.257562E-06	-3.89	0.04	-3.34	65.10
3-4, 84-86	63.34	0.5124137	1.068127E-06	-4.38	0.02	-3.83	65.60
3-5, 33-35	64.33	0.5124076	9.551653E-07	-4.50	0.02	-3.94	65.89
3-5, 66-68 S	64.66	0.5123963	1.360436E-06	-4.71	0.03	-3.98	65.99
3-5, 66-68	64.66	0.5124159	2.956583E-06	-4.33	0.06	-3.78	65.99
Site 883 B							
75-2, 20-22	714.03	0.5124750	3.16072E-06	-3.18	0.06	-2.89	34.73
76-1, 52-54	720.62	0.5125342	1.696093E-06	-2.02	0.03	-1.72	36.34
76-5, 94-96	727.04	0.5124859	3.431170E-06	-2.97	0.07	-2.65	37.91
77-1, 31-33	730.21	0.5125020	2.317680E-06	-2.65	0.05	-2.33	38.68
77-4, 50-52	734.90	0.5125042	2.116905E-06	-2.61	0.04	-2.28	39.82
78-3, 65-67 S	743.35	0.5127464	3.082797E-06	2.11	0.06	2.58	41.57
78-3, 65-67 L	743.35	0.5125952	6.404880E-07	-0.83	0.01	-0.40	41.57
79-2, 20-22	751.20	0.5125059	2.261971E-06	-2.58	0.04	-2.22	43.19
79-3, 65-67	753.15	0.5125021	2.012101E-06	-2.65	0.04	-2.29	43.59
82-1, 60-62	779.80	0.5125205	1.506023E-06	-2.29	0.03	-1.88	49.09
82-1, 60-62 R	779.80	0.5125310	1.529982E-06	-2.09	0.03	-1.68	49.09
82-7, 21-23	788.41	0.5125610	3.058178E-06	-1.50	0.06	-1.08	50.37
83-2, 75-77 S	791.45	0.5124647	8.013119E-07	-3.38	0.02	-2.81	50.63
83-2, 75-77 C	791.45	0.5125073	2.609515E-06	-2.55	0.05	-2.12	50.63
83-2, 75-77	791.45	0.5125167	2.952658E-06	-2.37	0.06	-1.94	50.63
83-2, 75-77 R	791.45	0.5125073	2.658458E-06	-2.55	0.05	-2.13	50.63
84-1, 75-77 C	799.95	0.5125186	2.631485E-06	-2.33	0.05	-1.90	51.37
84-1, 75-77	799.95	0.5125173	2.149999E-06	-2.35	0.04	-1.92	51.37
85-1, 60-62	809.50	0.5125060	2.085197E-06	-2.57	0.04	-2.14	52.20
85-4, 20-22	813.60	0.5124874	1.407876E-06	-2.94	0.03	-2.50	52.56
86-1, 20-22 S	818.70	0.5127240	1.592088E-06	1.68	0.03	2.31	56.59
86-1, 20-22 L	818.70	0.5127447	1.003080E-06	2.08	0.02	2.67	56.59

Core,Sec,Int	Depth (mbsf)	143/144	Std Error (abs)	ε_{Nd}	Error	$\varepsilon_{Nd}(t)$	Age (Ma)
86-2, 20-22	820.20	0.5127319	1.849921E-06	1.83	0.04	2.32	57.87
86-5, 5-7	824.55	0.5127992	1.507144E-06	3.14	0.03	3.66	61.60
87-1, 97-99	829.07	0.5127888	1.742943E-06	2.94	0.03	3.49	65.47
87-2, 75-77	830.25	0.5127298	2.156567E-06	1.79	0.04	2.35	66.49
Site 884 B							
74-5, 80-82 C	687.40	0.5125376	1.163335E-06	-1.96	0.02	-1.68	33.65
74-5, 80-82	687.40	0.5125249	1.736683E-06	-2.21	0.03	-1.92	33.65
74-5, 80-82 R	687.40	0.5125321	1.765805E-06	-2.07	0.03	-1.78	33.65
75-6, 45-47 C	698.15	0.5125007	2.206796E-06	-2.68	0.04	-2.39	34.48
75-6, 45-47	698.15	0.5124948	1.034097E-06	-2.79	0.02	-2.51	34.48
75-6, 45-47 R	698.15	0.5124958	1.731470E-06	-2.77	0.03	-2.48	34.48
77-6, 25-27	717.25	0.5124468	1.817301E-06	-3.73	0.04	-3.44	34.99
79-2, 78-80 S	731.08	0.5129642	3.132186E-06	6.36	0.06	6.76	35.36
79-2, 78-80 L	731.08	0.5129122	3.092330E-06	5.35	0.06	5.72	35.36
80-1, 85-87 S	739.25	0.5126370	2.672952E-06	-0.02	0.05	0.38	35.58
80-1, 85-87	739.25	0.5125491	7.195091E-07	-1.73	0.01	-1.44	35.58
82-1, 55-57	758.25	0.5125141	9.569891E-07	-2.42	0.02	-2.11	36.09
82-5, 70-72	764.40	0.5125292	2.127557E-06	-2.12	0.04	-1.82	36.25
83-2, 24-26	769.14	0.5125129	1.860260E-06	-2.44	0.04	-2.13	36.38
83-7, 28-30	776.03	0.5125156	1.562919E-06	-2.39	0.03	-2.08	36.56
84-5, 56-58	783.56	0.5125190	1.397511E-06	-2.32	0.03	-2.01	36.76
88-1, 100-102	816.60	0.5125084	1.325218E-06	-2.53	0.03	-2.21	37.64
89-1, 65-67	825.75	0.5125903	3.414520E-06	-0.93	0.07	-0.61	37.88
90-1, 93-95 S	835.53	0.5123935	1.038134E-06	-4.77	0.02	-4.34	38.14
90-1, 93-95	835.53	0.5124289	1.801646E-06	-4.08	0.04	-3.76	38.14
90-1, 93-95 R	835.53	0.5124337	1.500315E-06	-3.99	0.03	-3.67	38.14
Site 1208 A							
36-2, 3-5 S	326.43	0.5122740	1.134243E-06	-7.10	0.02	-6.55	49.77
36-2, 3-5	326.43	0.5123829	9.696347E-07	-4.98	0.02	-4.56	49.77
36-2, 15-17 C	326.55	0.5123874	2.003099E-06	-4.89	0.04	-4.47	50.16
36-2, 15-17	326.55	0.5123824	1.872277E-06	-4.99	0.04	-4.57	50.16
36-2, 28-30 S	326.68	0.5123873	1.009150E-06	-4.89	0.02	-4.32	50.58
36-2, 28-30 C	326.68	0.5123858	1.466031E-06	-4.92	0.03	-4.50	50.58
36-2, 28-30	326.68	0.5123932	1.783171E-06	-4.78	0.03	-4.35	50.58
36-2, 46-48	326.86	0.5124415	1.855713E-06	-3.83	0.04	-3.40	51.37
36-2, 46-48 R	326.86	0.5124394	1.666360E-06	-3.87	0.03	-3.44	51.37

Core,Sec,Int	Depth (mbsf)	143/144	Std Error (abs)	ε_{Nd}	Error	$\varepsilon_{Nd}(t)$	Age (Ma)
36-2, 55-57 S	326.95	0.5124189	2.909632E-06	-4.27	0.06	-3.70	51.62
36-2, 55-57	326.95	0.5124521	2.578741E-06	-3.63	0.05	-3.19	51.62
36-2, 88-90	327.28	0.5124306	7.226572E-07	-4.05	0.01	-3.61	52.54
36-2, 88-90 R	327.28	0.5124302	3.772446E-06	-4.05	0.07	-3.61	52.54
36-CC, 20-21 C	327.61	0.5124212	6.149054E-06	-4.23	0.12	-3.75	57.01
37-2, 40-42 C	336.40	0.5123929	9.223072E-06	-4.78	0.18	-4.26	62.03
38-2, 41-43 C	346.01	0.5124061	8.198498E-06	-4.52	0.16	-3.96	67.52
39-2, 40-42 C	355.70	0.5124248	8.198797E-06	-4.16	0.16	-3.55	73.06
40-2, 40-42 C	365.30	0.5123818	8.198109E-06	-5.00	0.16	-4.34	78.54
41-2, 40-42 C	375.00	0.5124265	9.223677E-06	-4.13	0.18	-3.42	84.09

VITA

Ashley Melissa Hague received a Bachelor of Science degree in Geology from Indiana University of Pennsylvania in May 2009. In August 2009, she entered the Geological Section of the Oceanography Department at Texas A&M University and graduated in August 2011 with a Master of Science degree in Oceanography. She can be reached at: Department of Oceanography, Texas A&M University, 3146 TAMU, College Station, TX 77843-3146 or via phone at: (979) 845-7211.